JOURNAL OF PETROLOGY | VOLUME 41 | NUMBER 4 | PAGES 477–509 | 2000

Trace Element Residence and Partitioning in Mantle Xenoliths Metasomatized by Highly Alkaline, Silicate- and Carbonate-rich Melts (Kerguelen Islands, Indian Ocean)

M. GRÉGOIRE[1], B. N. MOINE[2], SUZANNE Y. O'REILLY[1]*, J. Y. COTTIN[2] AND A. GIRET[2]

[1]GEMOC ARC NATIONAL KEY CENTRE, DEPARTMENT OF EARTH AND PLANETARY SCIENCES, MACQUARIE UNIVERSITY, NORTH RYDE, N.S.W. 2109, AUSTRALIA

[2]DEPARTMENT OF GEOLOGY–UMR 6524, UNIVERSITY J. MONNET, 23 RUE P. MICHELON, 42023 ST-ETIENNE, FRANCE

RECEIVED JANUARY 21, 1999; REVISED TYPESCRIPT ACCEPTED SEPTEMBER 21, 1999

Mantle xenoliths in alkaline lavas of the Kerguelen Islands consist of: (1) protogranular, Cr-diopside-bearing harzburgite; (2) poikilitic, Mg-augite-bearing harzburgite and cpx-poor lherzolite; (3) dunite that contains clinopyroxene, spinel phlogopite, and rarely amphibole. Trace element data for rocks and minerals identify distinctive signatures for the different rock types and record upper-mantle processes. The harzburgites reflect an initial partial melting event followed by metasomatism by mafic alkaline to carbonatitic melts. The dunites were first formed by reaction of a harzburgite protolith with tholeiitic to transitional basaltic melts, and subsequently developed metasomatic assemblages of clinopyroxene + phlogopite ± amphibole by reaction with lamprophyric or carbonatitic melts. We measured two-mineral partition coefficients and calculated mineral–melt partition coefficients for 27 trace elements. In most samples, calculated budgets indicate that trace elements reside in the constituent minerals. Clinopyroxene is the major host for REE, Sr, Y, Zr and Th; spinel is important for V and Ti; orthopyroxene for Ti, Zr, HREE, Y, Sc and V; and olivine for Ni, Co and Sc.

KEY WORDS: *mantle xenoliths; mantle metasomatism; partition coefficients; Kerguelen Islands; trace elements*

INTRODUCTION

Mantle xenoliths provide unique information about the chemistry and mineralogy of deep lithospheric rock types (e.g. Nixon, 1987; O'Reilly & Griffin, 1996). Studies of upper-mantle xenoliths in alkali basalts, kimberlites, lamproites and carbonatites have improved our understanding of materials and processes involved in the geochemical evolution of the mantle (e.g. Downes & Dupuy, 1987; Ionov *et al.*, 1993; Chalot-Prat & Boullier, 1997). The variation and magnitude of geochemical heterogeneities in the lithospheric mantle reflect the composition of mantle melts and fluids and the efficiency of heat and mass transfer. Mantle plumes are important for initiating such transfer processes. The Kerguelen plume is remarkable because of its volume, the persistence of volcanic activity for at least 115 My, and its migration across diverse geotectonic environments through time as a result of spreading of the Indian Ocean (Weis *et al.*, 1992).

In this paper we report a trace element study of bulk rocks and constituent minerals of clinopyroxene-bearing harzburgite, clinopyroxene-poor lherzolite and phlogopite + clinopyroxene-bearing dunite from the mantle beneath Kerguelen. These rocks show evidence for partial melting and mantle metasomatism related to the Kerguelen mantle plume. Our data yield insights into the distribution of trace elements in peridotites and concerning element partitioning between minerals under upper-mantle P–T conditions.

*Corresponding author. Telephone: +61-2-9850-8362. Fax: +61-2-9850-8428.
e-mail: sue.oreilly@mq.edu.au or soreilly@laurel.ocs.mq.edu.au

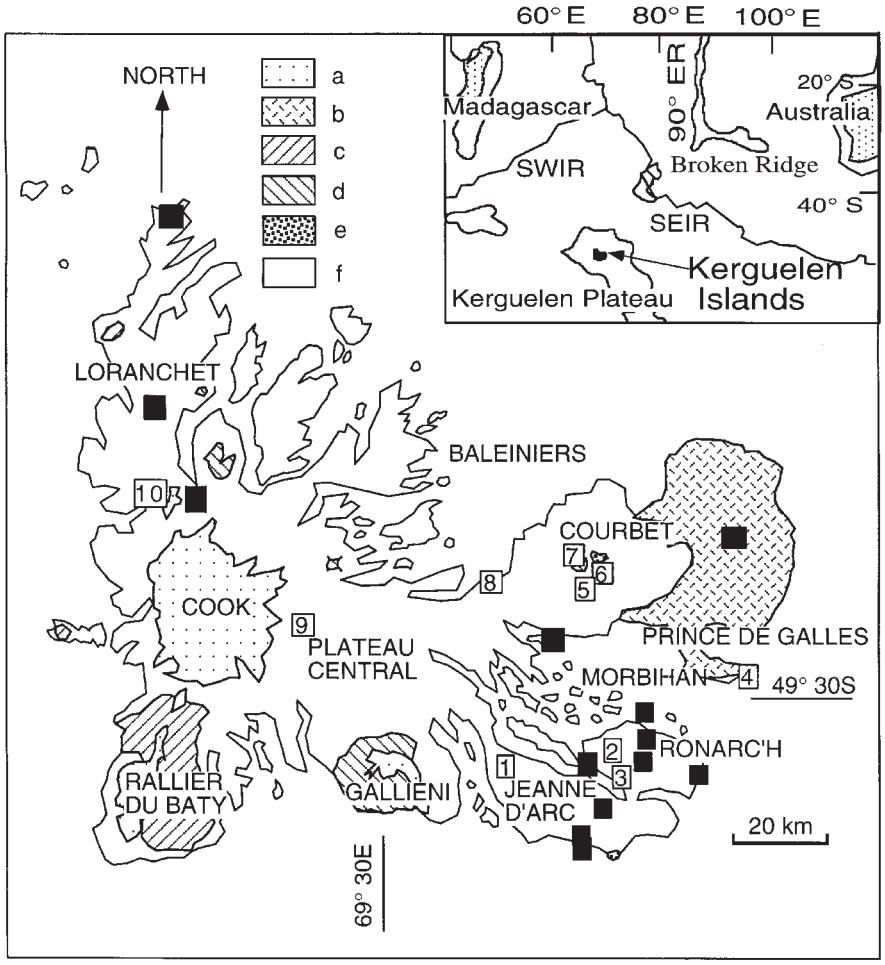

Fig. 1. Location of ultramafic and mafic xenolith-bearing alkali basalts of the Kerguelen Islands modified after Grégoire *et al.* (1997), a, Ice caps; b, moraines; c, alkaline silica-oversaturated volcano-plutonic complexes; d, alkaline silica-undersaturated volcano-plutonic complexes; e, tholeiitic-transitional plutonic complexes; f, flood basalts of transitional to alkaline type. Squares indicate ultramafic and mafic xenolith outcrops: numbered open squares refer to sample locality (see Appendix Table A1, for the naming of each outcrop); ■, other xenolith outcrops. Inset: location of Kerguelen Islands. SWIR, South West Indian Ridge; SEIR, South East Indian Ridge.

GEOLOGICAL SETTING

The Kerguelen Islands are located in the oceanic domain of the Antarctic Plate (Fig. 1). They are the exposed part of the Kerguelen oceanic plateau, which is the second largest (25×10^6 km^3) after the Ontong Java plateau (Coffin & Eldhom, 1993). The Kerguelen Islands drifted from a location near the South East Indian Ridge (SEIR) to their present-day intraplate setting. Their magmatic activity has extended over 45 My (Giret, 1993). Therefore, the Kerguelen Islands combine characteristics of both the Iceland and Hawaiian hotspots (Giret *et al.*, 1997). Magmatism has progressively changed from tholeiitic to alkaline (Gautier *et al.*, 1990; Weis *et al.*, 1993).

Ultramafic and mafic xenoliths from the Kerguelen Islands are found in dykes, lava flows and breccia pipes of the youngest and more alkaline basaltic rocks (Grégoire *et al.*, 1994, 1998; Mattielli *et al.*, 1996). We collected xenoliths from 10 different localities in the archipelago (Fig. 1). The xenoliths are subrounded in shape and range from 10 to 20 cm. They are Type I Kerguelen mantle xenoliths of Grégoire *et al.* (1997).

SAMPLING AND ANALYTICAL METHODS

Samples (50–100 g) from the central parts of xenoliths were ground in an agate mill. Major and minor elements (Cr, Ni) in bulk rocks were analysed by X-ray fluorescence spectrometry (XRF) at Macquarie University [see O'Reilly & Griffin (1988) for methods]. The concentrations of 29 minor and trace elements [rare earth

elements (REE), Ba, Rb, Th, U, Nb, Ta, Pb, Sr, Zr, Ti, Y, Sc, V, Co, Cu and Zn] were analysed by inductively coupled plasma mass spectrometry (ICP-MS) with a Perkin Elmer Sciex Elan 6000 instrument at Macquarie University. The sample preparation for ICP-MS was as follows: 100 mg of sample powder was dissolved in concentrated HF–HNO_3 in 17 ml Savillex Teflon screw-top beakers. Following digestion, samples were evaporated to incipient dryness, dissolved in 6 N HNO_3, and again evaporated to incipient dryness. Remaining residues were dissolved in 2% HNO_3. The sample solutions were transferred to 125 ml polypropylene bottles. A known weight of internal standard solution was added and the solution was diluted with 2% HNO_3. Final sample/solution ratios were ~1000–1200. The technique yields results that agree well with recommended values for the Kilauea basalt KIL-1 [93-1489 of Eggins *et al.* (1997)], which was used as a standard, and also measured along with the samples to assess precision (<2·5% RSD). The reference standard W-1 was prepared and analysed with the samples, together with three reagent blanks. No oxide corrections were used. Detection limits (taking into account chemical blank) were 1–5 ppb for most REE, Y, Nb, Ta, Th and U; 5–30 ppb for Ce, Sm, Zr, Rb, Sr, Ba, Pb and Sc; 50–100 ppb for V and Co; 200 ppb for Cu and Zn; and 500 ppb for Ti.

Mineral compositions were determined by a Cameca Camebax SX 50 microprobe at Macquarie University using wavelength-dispersive spectrometry (WDS). The microprobe was used with 15 kV accelerating voltage, sample current of 20 nA, a beam diameter of 2–3 mm, and natural and synthetic minerals as standards. Matrix corrections were done by PAP (Pouchou & Pichoir, 1984) procedures. Count times were 20–40 s and no values are reported below detection limits (0·01–0·04 wt %).

Concentrations of 29 trace elements (REE, Ba, Rb, Th, U, Nb, Ta, Pb, Sr, Zr, Hf, Ti, Y, Sc, V, Co and Ni) and of Al and Ca in olivine were determined in >100 mm polished sections by ICP-MS with a Perkin Elmer Elan 5100 instrument (16 samples) and a Perkin Elmer Elan 6000 instrument (three samples) at Macquarie University. Both ICP instruments were coupled to a Continuum Surelite I-20, Q-switched Nd:YAG laser ablation system (LA-ICP-MS). A typical analysis consists of 120 replicates, with each replicate representing one sweep of the mass range at a dwell time of 50–100 ms per mass. For each sample, 30–35 replicates were counted on the carrier gas (argon) alone to establish the background, followed by 85–90 replicates for ablation. The NIST 610 glass standard was used to calibrate relative element sensitivities. Each analysis was normalized using either CaO (clinopyroxene) or MgO (orthopyroxene, olivine, spinel, phlogopite, amphibole) values determined by electron microprobe. Typical detection limits are in the range 10–20 ppb for REE, Ba, Rb, Th, U, Nb, Ta, Pb, Sr, Zr, Hf and Y; 100 ppb for V and Sc; 2 ppm for Ti, Ni, Co and Cr; and 5 ppm for Al and Ca. The typical precision and accuracy for a laser microprobe analysis range from 2 to 7%. A more detailed description of laser operating conditions, calibration values for the NIST 610 glass standard and error analysis have been given by Norman *et al.* (1996) and Norman (1998). The LAMTRACE program developed by S. E. Jackson (e.g. Longerich *et al.*, 1996) was used for data reduction.

Modal compositions (Table 1) were calculated by mass balance based on major element bulk-rock compositions and electron-microprobe analyses of constituent minerals.

PETROGRAPHY AND MODAL COMPOSITION

Protogranular and poikilitic harzburgite xenoliths show local gradation to porphyroclastic microstructures in which a fine-grained mosaic of olivine and orthopyroxene neoblasts (<1 mm) surrounds larger porphyroclasts (2–10 mm). Crystals in protogranular harzburgites show curvilinear grain boundaries. The grain size of olivine and orthopyroxene typically varies from 2 to 10 mm. The poikilitic texture is similar to that described for some harzburgitic xenoliths from the French Massif Central (Coisy & Nicolas, 1978). Poikilitic microstructure differs from the protogranular microstructure by the presence of olivine grains up to 5 cm long that contain inclusions of orthopyroxene. Clinopyroxene grains typically contain inclusions of resorbed orthopyroxene and spinel grains. Vermicular spinel grains in both types of harzburgites occur between olivine and pyroxene crystals and frequently form clusters with orthopyroxene and clinopyroxene. Phlogopite rarely occurs only in poikilitic harzburgites. Millimetre-sized interstitial phlogopite crystals contain inclusions of spinel, olivine and orthopyroxene, and are in textural equilibrium with clinopyroxene. More rarely, phlogopite forms thin veins (<0·5 mm). Amphibole was found in a single sample (OB-93-5) of phlogopite-bearing harzburgite. Most of the amphibole grains are rounded interstitial, but a few occur as inclusions in phlogopite grains. Clinopyroxene-bearing harzburgite and clinopyroxene-poor lherzolite xenoliths from the Kerguelen Islands contain melt and fluid inclusions trapped in olivine and pyroxene (Schiano *et al.*, 1994). Poikilitic samples are especially rich in such inclusions.

Clinopyroxene + phlogopite-bearing dunite samples are coarse-grained rocks made up mostly of 2–5 (rarely to 10) mm olivine grains. Clinopyroxene, orthopyroxene, spinel, phlogopite and amphibole grains range from 0·1 to 2 mm. Small, isolated, globular to anhedral grains of spinel are either interstitial or occur as inclusions in olivine, or more rarely, in clinopyroxene. Clinopyroxene

Table 1: Representative bulk-rock major element abundances and calculated modal compositions (see text) of type I mantle xenoliths from the Kerguelen Islands

Sample:	OB-93-58	OB-93-279	OB-93-426	OB-93-22	GM-92-501	OB-93-3	OB-93-5	JGM-92-1c	GM-92-480	BOB-93-640.1	MM-94-101
ol:	79	76	71	70	68	67	74	79	96	94	97
opx:	19	19	26	26	27	29	21	13	—	—	—
cpx:	1·5	4	2·5	3·5	4·5	3	3·5	7	1·5	3	1·5
sp:	0·5	1	0·5	0·5	0·5	0·5	0·5	1	2	2	1
phl:	—	—	—	—	—	0·5	0·5	—	0·5	1	0·5
am:	—	—	—	—	—	—	0·5	—	—	—	—
SiO_2	43·25	43·85	44·90	44·55	44·65	44·50	43·40	42·40	39·60	38·75	39·75
TiO_2	—	—	0·01	0·01	0·17	0·04	0·08	0·16	0·04	0·05	0·05
Al_2O_3	0·50	0·90	0·80	1·05	1·50	1·40	1·25	1·20	0·80	0·70	0·45
MgO	46·05	44·40	44·80	43·90	43·40	44·15	44·20	42·80	45·15	42·60	45·50
FeO	7·40	7·45	7·20	8·15	7·80	7·65	7·45	10·40	11·95	12·15	11·90
MnO	0·09	0·12	0·12	0·10	0·11	0·12	0·11	0·13	0·15	0·16	0·13
CaO	0·65	0·70	0·75	0·70	0·95	0·85	0·80	1·30	0·35	0·50	0·40
Na_2O	0·07	0·05	0·10	0·15	0·25	0·15	0·15	0·25	0·20	0·15	0·20
K_2O	—	—	0·01	0·01	0·07	0·05	0·09	0·02	0·01	0·01	0·02
P_2O_5	—	—	—	—	0·04	0·03	0·05	0·03	0·02	0·01	0·01
H_2O^+	0·65	1·60	0·95	0·95	0·65	0·45	1·10	0·40	0·60	1·75	0·65
H_2O^-	0·09	0·20	0·13	0·21	0·22	0·13	0·25	0·02	0·23	0·25	0·15
CO_2	0·20	0·09	0·10	0·13	0·05	0·06	0·10	0·09	0·07	2·25	0·85
Total	98·95	99·36	99·87	99·91	99·86	99·58	99·03	99·20	99·17	99·33	100·06
mg-no.	91·73	91·39	91·73	90·57	90·84	91·14	91·36	88·01	87·07	86·21	87·21

Phl, phlogopite; opx, orthopyroxene; cpx, clinopyroxene; sp, spinel; am, amphibole. *mg*-number = 100Mg/(Mg + Fe_{total}) on an atomic basis.

is interstitial and locally concentrated in thin layers (<0·5 mm) between olivine crystals. Clinopyroxene commonly contains exsolution lamellae of spinel. Phlogopite grains are commonly euhedral and interstitial but some are found as inclusions in olivine. Sample MG-91-143 contains both amphibole and phlogopite. The amphibole is interstitial and commonly appears to have replaced interstitial clinopyroxene. Samples MM-94-54, MM-94-97 and MM-94-101 contain numerous sulphide mineral grains.

Protogranular and poikilitic harzburgite samples contain 67–84% olivine, 13–29% orthopyroxene, 1·5–5% clinopyroxene and 0·5–1·5% spinel. Phlogopite (0·5%) is present in samples OB-93-3 and OB-93-5, and amphibole (0·5%) in sample OB-93-5. Poikilitic sample JGM-92-1c is the first true lherzolite reported from the Kerguelen Islands [according to Streckeisen's (1976) classification]. It is poor in clinopyroxene (olivine 79%, orthopyroxene 13%, clinopyroxene 7%, spinel 1%). Kerguelen dunites (olivine 94–97%) contain 1–3% of clinopyroxene and 1–2% of spinel. Phlogopite (0·5–1·5%) is found in all dunite samples, whereas amphibole has been observed in only one sample (MG-91-143).

Many samples display interstitial patches and/or veins of fine-grained material with a complex mineralogy. In harzburgite samples OB-93-3, OB-93-5, GM-92-501 and GM-92-502, this material consists of feldspar + olivine2 + rutile + ilmenite + Cr-armalcolite + Cr–Ca-armalcolite + Ti-chromite. Other samples of harzburgite and dunite display patches <50 μm wide that consist of clinopyroxene2 ± olivine2 ± amphibole ± biotite ± chromite ± ilmenite ± rutile ± feldspar ± carbonate ± glass. Electron microprobe analyses show that compositional effects of these assemblages on the original minerals of the host peridotite are restricted to the adjacent 50–100 μm of host minerals.

MAJOR ELEMENT COMPOSITION

Whole-rock samples

The protogranular and poikilitic harzburgites and clinopyroxene-poor lherzolite have similar major element

contents, with CaO/Al_2O_3 ratios that range from 0·60 to 1·30 (Table 1). All are strongly depleted in 'basaltic' components (CaO <1·35 wt %; Al_2O_3 <1·45 wt %; Na_2O <0·25 wt %) compared with model compositions for the undepleted upper mantle (CaO 3·23–3·60 wt %; Al_2O_3 4–4·46 wt %; Na_2O 0·33–0·61 wt %, Jagoutz *et al.*, 1979; McDonough & Sun, 1995). However, protogranular harzburgite samples display *mg*-numbers [100Mg/(Mg + Fe^{2+})] of 91·4–92, higher than that for primitive upper mantle (89·8). The *mg*-numbers of poikilitic harzburgite samples vary from 89·9 to 91·8, and poikilitic, clinopyroxene-poor lherzolite sample JGM-92-1c has an *mg*-number of 88.

Dunite samples exhibit low CaO (0·24–0·53 wt %), Na_2O (0·15–0·21 wt %), Al_2O_3 (0·44–0·82 wt %) and TiO_2 (0·04–0·07 wt %) contents, which suggest a refractory character, but their *mg*-numbers (86–88·5) are lower than those for both primitive mantle (89·8) and the harzburgite xenoliths. The CaO/Al_2O_3 ratios of dunite samples are 0·40–0·89.

Minerals in clinopyroxene-bearing harzburgite

The *mg*-numbers of olivine range from 86 to 92 in the two types of harzburgite. Olivine compositions are more uniform in protogranular harzburgites (*mg*-number = 90·5–92) than in poikilitic peridotites (*mg*-number = 86–92). The lowest *mg*-number value is for olivine from lherzolite sample JGM-92-1c. Orthopyroxene displays a similar distribution. Clinopyroxene *mg*-numbers range from 91·5 to 92·5 in protogranular harzburgite samples, and from 87·5 to 92·5 in poikilitic ones (Table 2). Orthopyroxene from poikilitic harzburgite samples is typically richer in Na_2O, Al_2O_3 and TiO_2 than those of protogranular harzburgites (Table 2).

Clinopyroxene ranges in composition from diopside in protogranular harzburgite samples to magnesian augite in poikilitic harzburgites and lherzolite samples (Table 2). The *mg*-number of diopside is high and homogeneous (93–95) for protogranular harzburgite, but shows a wider range and lower values (86–91·5) for harzburgite and lherzolite samples that contain poikilitic Mg-augite. The *mg*-number of clinopyroxene is systematically higher than those of olivine and orthopyroxene in protogranular harzburgite samples. In contrast, the *mg*-number of the clinopyroxene from poikilitic, Mg-augite harzburgite and lherzolite samples is lower than or equal to that of olivine and orthopyroxene. The Mg-augite is richer in Al_2O_3, Na_2O, TiO_2 and Cr_2O_3 than is Cr-diopside from protogranular harzburgite samples (Table 2).

Spinel grains are Mg–Al chromites that display *mg*-numbers of 66·5–72 and *cr*-numbers [100Cr/(Cr + Al)] of 40–52 in protogranular harzburgite samples, and *mg*-numbers of 58–79 and *cr*-numbers of 20–49 in poikilitic harzburgite and lherzolite samples. The TiO_2 contents of spinel are smaller in protogranular harzburgite samples (<0·07 wt %) than in poikilitic harzburgite and lherzolite samples (0·20–2·80 wt %).

The amphibole in poikilitic harzburgite sample OB-93-5 is pargasite of fairly constant TiO_2, Na_2O and Cr_2O_3 contents (Table 2)

The phlogopite in poikilitic harzburgite samples OB-93-3 and OB-93-5 displays high *mg*-numbers and Cr_2O_3 contents (Table 2).

Minerals in clinopyroxene + phlogopite-bearing dunite

The *mg*-numbers of olivine in dunite samples range from 86 to 90. These samples contain an Al–Cr diopside in which *mg*-numbers range from 87·5 to 90 (Table 2). Spinel is Mg-chromite that shows a wide range of composition and significant amounts of Fe_2O_3 and TiO_2 (Table 2). Phlogopite (*mg*-number 85–90) has Cr_2O_3 of 1·40–2·20 wt %. Phlogopite associated with amphibole in sample MG-91-143 has less TiO_2, Al_2O_3 and K_2O, and more Na_2O and SiO_2 than that found in amphibole-free dunite samples (Table 2). The disseminated amphibole in sample MG-91-143 (*mg*-number 84·75) is pargasite (Table 2).

Equilibration temperatures

Equilibration temperatures of clinopyroxene-bearing harzburgite and clinopyroxene-poor lherzolite samples were estimated using two-pyroxene geothermometers (Brey & Köhler, 1990*a*), the Ca-in-orthopyroxene geothermometer (Brey & Köhler, 1990*b*), orthopyroxene–spinel equilibria (Sachtleben & Seck, 1981) and olivine–spinel equilibria (Fabriès, 1979; Ballhaus *et al.*, 1991). Core compositions of large grains in the harzburgites were used. Our goal was only to establish relative temperatures that are consistently estimated by all methods.

The majority of the mineral assemblages in the protogranular harzburgite samples re-equilibrated at T = 845–1005°C (Table 3). The range of equilibration temperatures is systematically higher for poikilitic harzburgite and cpx-poor lherzolite samples (T = 1015–1135°C). The olivine–spinel and orthopyroxene–spinel geothermometers yield temperatures of 925–940°C for sample GM-92-502.

In samples of clinopyroxene + phlogopite-bearing dunite, the absence of orthopyroxene makes temperature estimates less reliable. Olivine–spinel equilibria yield equilibration temperatures of 940–1090°C (Table 3).

Table 2: Representative electron microprobe analyses of minerals from Kerguelen harzburgites, cpx-poor lherzolite and dunites (average values)

Sample:	OB-93-58				OB-93-279				OB-93-426				OB-93-22				GM-92-501		
	cpx	opx	ol	sp	cpx	opx	ol	sp	cpx	opx	ol	sp	cpx	opx	ol	sp	cpx	opx	ol
n:	5	5	3	2	12	7	5	3	9	13	6	2	6	18	9	4	2	3	8
SiO_2	53·80	56·95	41·00	0·07	53·65	56·85	41·00	0·03	54·00	56·95	41·25	0·04	53·05	55·70	40·55	0·09	52·00	55·15	40·70
TiO_2	—	0·01	0·03	0·04	0·02	0·01	0·01	0·01	0·03	0·02	0·01	0·04	0·13	0·06	0·01	0·23	0·70	0·24	0·03
Al_2O_3	1·81	1·89	0·01	28·45	2·01	2·13	0·02	31·15	2·25	2·14	0·01	28·10	3·56	2·89	0·15	30·50	5·00	3·68	0·03
Cr_2O_3	0·78	0·48	0·04	39·90	0·76	0·54	0·02	38·19	0·96	0·59	0·02	41·10	1·24	0·73	0·04	36·20	1·35	0·74	0·03
NiO	0·07	0·12	0·44	0·30	0·08	0·12	0·41	0·18	0·06	0·09	0·39	0·18	0·05	0·12	0·41	0·21	0·03	0·11	0·40
MgO	18·10	35·05	50·60	16·45	17·55	34·55	50·25	16·50	17·75	34·60	50·65	16·15	17·65	33·40	49·20	16·65	16·20	33·65	50·30
FeO	2·15	5·20	8·18	13·40	1·97	5·60	8·80	12·60	2·19	5·31	8·45	13·55	3·10	5·97	9·39	14·60	3·10	6·01	9·13
MnO	0·07	0·11	0·15	—	0·08	0·13	0·15	—	0·07	0·13	0·12	—	0·08	0·10	0·12	—	0·10	0·15	0·13
CaO	23·05	0·75	0·07	0·02	23·85	0·73	0·06	0·01	22·65	0·81	0·06	0·02	19·70	1·28	0·28	0·02	19·90	0·96	0·13
Na_2O	0·27	0·02	—	0·01	0·20	—	0·01	0·01	0·47	0·03	0·01	0·02	1·06	0·13	0·02	0·01	1·36	0·11	0·01
K_2O	0·01	—	—	0·01	0·01	—	0·01	—	0·01	—	0·01	0·01	0·01	0·01	0·02	—	0·01	—	—
Total	100·10	100·57	100·51	98·63	100·16	100·66	100·74	98·68	100·43	100·66	100·97	99·19	99·62	100·39	100·19	98·48	99·75	100·78	100·87
mg-no.	93·76	92·32	91·68	68·59	94·09	91·67	91·04	70·01	93·52	92·08	91·44	67·97	91·02	90·89	90·32	67·07	90·31	90·90	90·76
cr-no.				48·48				45·13				49·52				44·33			

Sample:	GM-92-501		OB-93-3				OB-93-5						JGM-92-1c			
	sp	cpx	opx	ol	sp	phl	cpx	opx	ol	sp	phl	am	cpx	opx	ol	sp
n:	2	4	5	5	2	3	12	21	11	7	12	15	4	5	12	2
SiO_2	0·13	52·30	56·05	40·65	0·08	37·85	51·60	55·45	40·65	0·07	37·10	42·35	50·20	54·80	40·55	0·10
TiO_2	2·55	0·42	0·04	0·01	0·51	4·97	0·56	0·11	0·01	0·32	4·37	2·93	1·30	0·43	0·02	1·68
Al_2O_3	34·20	5·31	2·84	0·03	35·35	16·00	6·24	3·50	0·02	46·40	16·55	13·55	5·94	3·97	0·04	35·95
Cr_2O_3	29·50	1·47	0·57	0·04	31·35	1·86	1·36	0·49	0·04	20·19	1·84	2·01	1·27	0·63	0·04	25·56
NiO	0·29	0·04	0·12	0·41	0·21	0·20	0·04	0·11	0·42	0·35	0·21	0·12	0·06	0·09	0·37	0·30
MgO	17·70	16·35	34·15	50·45	17·75	20·40	15·75	33·95	50·50	19·90	20·55	16·85	15·15	31·65	47·30	16·40
FeO	14·32	3·03	5·63	8·93	13·70	4·10	2·77	5·33	8·31	11·14	3·79	3·59	4·15	7·80	12·55	18·85
MnO	—	0·06	0·13	0·12	—	0·01	0·08	0·11	0·12	—	—	0·04	0·11	0·17	0·16	—
CaO	0·02	19·05	0·84	0·09	0·02	0·02	19·00	0·87	0·08	0·01	0·02	10·30	18·90	1·17	0·16	0·03
Na_2O	0·02	1·69	0·13	0·02	0·01	0·76	1·87	0·16	0·01	0·02	0·84	2·97	1·56	0·14	0·02	0·02
K_2O	0·01	0·01	0·01	0·01	—	9·38	0·01	0·01	0·01	0·01	9·13	1·65	—	0·01	0·01	0·01
Total	98·72	99·71	100·49	100·70	98·94	95·57	99·27	100·12	100·20	98·42	94·41	96·38	98·84	100·81	101·22	98·86
mg-no.	68·85	90·59	91·54	90·97	69·74	89·86	91·00	91·91	91·55	76·10	90·61	89·30	86·69	87·86	87·03	60·83
cr-no.	36·66				37·30					22·60						32·29

Table 2: continued

Sample:	GM-92-480				BOB-93-601.1				MM-94-101				MG-91-143				
	ol	cpx	phl	sp	ol	cpx	phl	sp	ol	phl	cpx	sp	ol	cpx	am	phl	sp
n:	19	8	6	9	6	10	3	2	15	9	6	4	2	5	5	4	2
SiO_2	40·40	52·05	37·45	0·07	40·25	52·80	36·75	0·03	39·65	37·10	52·10	0·06	40·50	52·50	45·20	40·45	0·02
TiO_2	0·02	0·61	4·16	0·78	—	0·52	4·73	0·98	0·01	5·38	0·58	1·00	0·01	0·55	1·19	1·50	0·51
Al_2O_3	0·03	5·20	15·97	34·41	0·02	3·38	15·40	27·20	0·01	15·40	4·23	27·80	0·01	4·16	10·70	14·90	13·35
Cr_2O_3	0·05	1·26	1·59	27·89	0·03	0·83	1·51	34·00	0·05	2·01	1·43	36·10	0·03	2·06	2·36	2·19	44·80
NiO	0·38	0·04	0·19	0·30	0·31	0·03	0·17	0·17	0·33	0·21	0·03	0·22	0·35	0·04	0·10	0·19	0·22
MgO	48·30	14·85	20·30	16·20	46·45	16·10	19·55	12·70	47·40	19·40	15·20	13·90	46·30	14·50	17·35	22·25	9·53
FeO	11·02	3·39	5·02	18·45	13·35	3·87	5·75	22·55	12·25	5·33	3·51	19·25	13·05	3·72	5·57	5·88	28·50
MnO	0·16	0·04	0·02	—	0·19	0·08	—	—	0·17	0·01	0·07	—	0·17	0·04	0·06	0·01	—
CaO	0·14	20·35	0·01	—	0·07	21·20	0·07	—	0·07	0·01	19·70	0·01	0·05	19·85	9·56	0·02	0·01
Na_2O	0·02	1·86	0·62	0·01	0·03	1·08	0·84	0·01	0·01	0·88	1·85	0·01	0·02	2·00	4·06	1·21	0·02
K_2O	0·01	0·01	9·52	0·01	0·02	0·01	8·79	0·01	—	9·04	0·01	0·01	0·02	0·01	0·98	8·07	—
Total	100·52	99·65	94·85	98·11	100·72	99·91	93·56	97·64	99·95	94·76	98·72	98·35	100·50	99·43	97·14	96·68	96·95
mg-no.	88·65	88·66	87·81	60·98	86·10	88·10	85·82	50·10	87·35	86·65	88·51	56·29	86·35	87·41	84·73	87·08	37·34
cr-no.				35·22				45·61				46·56					69·25

Ol, olivine; cpx, clinopyroxene; opx, orthopyroxene; sp, spinel; phl, phlogopite; am, amphibole. *mg*-number = 100Mg/(Mg + Fe_{total}); *cr*-number = 100Cr/(Cr + Al).

Table 3: Equilibration temperatures of the Kerguelen mantle peridotite xenoliths; when required, assumed pressure is 1·5 GPa

Sample	B&K(1990*a*) Two-pyroxenes	B&K(1990*b*) Ca in orthopyroxene	S&S(1981)	F(1979)	B(1991)
OB-93-58	910	995	905	1005	1000
OB-93-279	845	970	860	980	1000
BOB-93-666	855	945	880	900	900
OB-93-426	910	1000	965	975	990
OB-93-67b	935	995	930	1000	1005
OB-93-22	1135	1125	1065	1035	1035
GM-92-453	1125	1070	1125	1040	1030
GM-92-502	1065	1040	930	940	925
GM-92-501	1080	1045	1070	1040	1040
OB-93-3	1105	1015	1015	1030	1030
OB-93-5	1100	1025	1020	1025	1025
JGM-92-1c	1080	1090	1075	1100	1060
GM-92-468	—	—	—	1050	1025
GM-92-480	—	—	—	1090	1030
BOB-93-640.1	—	—	—	985	940
MM-94-54	—	—	—	1005	980
MM-94-97	—	—	—	990	970
MM-94-101	—	—	—	985	965

B&K(1990*a*), Brey & Köhler (1990*a*); B&K(1990*b*), Brey & Köhler (1990*b*); S&S(1981), Sachtleben & Seck (1981); F(1979), Fabriès (1979); B(1991), Ballhaus *et al.* (1991).

TRACE ELEMENT COMPOSITIONS

Transition trace elements in clinopyroxene-bearing harzburgite and clinopyroxene-poor lherzolite

The harzburgites and the clinopyroxene-poor lherzolite show very similar bulk-rock transition element contents (Table 4). They are samples richer in Ni and Co, and poorer in Sc and V than the postulated primitive upper mantle (Table 4; McDonough & Sun, 1995).

Olivine (Table 5) and spinel (Table 6) from protogranular harzburgite samples are respectively poorer in Cr and Ni than those from poikilitic harzburgite and lherzolite samples. Ca and Al contents of olivine are greater and vary more widely in poikilitic than in protogranular harzburgite samples (Table 5). Orthopyroxene shows the most marked difference in composition between the two textural types. Sc is higher and Co and Ni are commonly lower in protogranular harzburgite samples than in poikilitic peridotite samples (Table 7). There is no systematic difference in the transition trace element content of the Cr-diopside occurring in the protogranular harzburgite samples and of the Mg-augites in the poikilitic peridotite samples, but the latter display a wider range of compositions (Table 8). Spinel and phlogopite (Tables 6 and 9) of Kerguelen harzburgites and clinopyroxene-poor lherzolite are rich in V and Co and poor in Sc. Sc is concentrated in clinopyroxene (45–73 ppm) and amphibole (47 ppm) (Tables 8 and 9).

Transition trace elements in clinopyroxene + phlogopite-bearing dunite

Dunites have bulk-rock Ni, Sc and V contents similar to those of harzburgites; the two samples rich in sulphides (MM-94-51 and MM-94-101) are higher in Cu (Table 4). Clinopyroxene grains in dunite are richer in Sc than those of harzburgites (Table 8). Olivine (Table 5) from dunites displays the same Cr contents as those from protogranular harzburgite. Its Ca and Al contents vary in a range, which approximately covers those of the two types of harzburgites. Ni/Co ratios of dunitic olivine range from 12·3 to 19·85, and are typically below the primitive mantle value of 18 (McDonough & Sun, 1995) and lower than those of the two types of harzburgites

Table 4: Representative bulk-rock trace element compositions of type I mantle xenoliths from the Kerguelen Islands (values in ppm)

Sample:	OB-93-58	OB-93-279	OB-93-426	OB-93-22	GM-92-501	OB-93-3	OB-93-5	JGM-92-1c	GM-92-480	BOB-93-640.1	MM-94-101
Sc	7·72	11·03	10·29	8·88	9·75	8·56	8·79	7·61	5·12	6·24	6·15
V	22·9	47·9	30·3	30·3	48·5	30·4	30·1	43·0	29·1	34·3	19·4
Cr (XRF)	2399	2626	3028	2530	2424	3135	1310	2601	4405	3796	2482
Co	141	137	137	137	142	135	126	145	185	195	198
Ni (XRF)	2582	2354	2385	2417	2379	2399	2474	2331	2690	1955	2549
Cu	5·1	8·4	5·1	3·8	22·5	4·6	7·1	8·6	3·1	10·3	58·1
Zn	43·6	43·4	43·4	50·8	71·0	53·5	46·1	100·3	101·0	86·4	77·3
Rb	0·264	0·372	0·183	0·952	1·315	3·872	4·648	0·535	0·603	0·403	0·718
Ba	0·267	0·162	0·208	5·010	9·978	6·547	14·253	3·458	2·357	3·686	4·886
Sr	19·20	2·687	5·312	14·21	25·56	29·73	61·53	17·05	9·410	8·890	7·870
Pb	0·163	0·144	0·126	0·141	0·379	0·142	0·331	0·228	0·133	0·108	0·207
Th	0·009	0·015	0·026	0·135	0·351	0·117	0·365	0·109	0·014	0·044	0·052
U	0·001	0·002	0·006	0·066	0·106	0·049	0·079	0·017	0·002	0·009	0·009
Nb	0·026	0·063	0·177	0·476	2·708	0·887	2·727	0·403	0·221	0·369	0·469
Ta	0·001	0·003	0·010	0·058	0·167	0·079	0·124	0·045	0·023	0·036	0·034
Ti	9·12	23·3	97	107	1268	282	530	1112	318	358	326
Zr	0·089	0·413	1·190	3·791	10·34	12·33	11·34	8·68	2·455	2·544	3·580
La	0·013	0·033	0·151	0·669	2·728	1·332	3·283	1·266	0·113	0·409	0·366
Ce	0·016	0·065	0·288	1·217	4·688	3·607	6·365	2·633	0·358	0·808	0·788
Pr	0·002	0·008	0·034	0·133	0·517	0·484	0·717	0·406	0·058	0·098	0·100
Nd	0·007	0·032	0·131	0·471	1·857	2·118	2·567	1·943	0·279	0·379	0·411
Sm	0·001	0·007	0·028	0·076	0·360	0·473	0·446	0·521	0·073	0·072	0·093
Eu	0·001	0·002	0·009	0·023	0·106	0·146	0·127	0·166	0·023	0·024	0·029
Gd	0·001	0·005	0·028	0·072	0·359	0·463	0·398	0·564	0·071	0·066	0·100
Tb	0·001	0·001	0·005	0·010	0·054	0·068	0·056	0·083	0·010	0·010	0·016
Dy	0·001	0·006	0·027	0·051	0·279	0·371	0·287	0·458	0·054	0·056	0·086
Ho	0·001	0·002	0·007	0·010	0·052	0·075	0·055	0·089	0·011	0·011	0·018
Er	0·001	0·006	0·021	0·029	0·139	0·202	0·149	0·229	0·032	0·034	0·052
Yb	0·005	0·019	0·028	0·033	0·123	0·188	0·137	0·189	0·033	0·040	0·053
Lu	0·002	0·004	0·005	0·006	0·019	0·029	0·022	0·029	0·007	0·008	0·010
Y	0·011	0·038	0·156	0·289	1·328	1·767	1·772	2·080	0·230	0·268	0·420

Cr and Ni have been analysed by XRF and other elements by ICP-MS (see text for methods).

(19·4–22). Spinel in Kerguelen dunites is also rich in V, Co and Ni, and contains little Sc (Table 6). Phlogopite (Table 9) in amphibole-bearing dunite contains less Sc and V than in amphibole-free samples. Amphibole in the phlogopite-bearing sample (Table 9) contains significant amounts of Sc, V, Co and Ni.

Incompatible trace elements (REE, Y, HFSE, LILE)

The two types of harzburgites and the lherzolite from Kerguelen have different incompatible trace element characteristics, but all are enriched in the more incompatible trace elements (Table 4; Figs 2 and 3). Both clinopyroxene grains and bulk-rock samples display U-shaped REE patterns in protogranular harzburgite and light REE (LREE)-enriched REE patterns in poikilitic harzburgite and lherzolite (Figs 2 and 3). In Kerguelen dunite samples, only the Rb and Pb values of bulk-rock analyses (and Th in sample MM-94-54) are close to those of primitive mantle. Other elements are significally depleted relative to the primitive mantle (Fig. 4). Dunite samples display trace element patterns enriched in the more incompatible trace elements (Fig. 4). Olivine and

Table 5: Representative olivine trace element analyses (LA-ICP-MS) from type I mantle xenoliths from the Kerguelen Islands (values in ppm)

Sample:	OB-93-58	OB-93-279	OB-93-426	OB-93-22	GM-92-501	OB-93-3	OB-93-5	JGM-92-1c	GM-92-480	BOB-93-640.1	MM-94-101	MG-91-143
n:	2	2	2	2	2	2	2	2	2	2	2	2
Al	137	53	72	231	369	231	223	339	208	369	89	37
Ca	556	600	469	741	1215	725	791	986	702	353	389	536
Sc	3·0	3·3	4·2	2·3	3·2	2·6	3·1	3·1	4·8	3·5	4·5	2·2
V	3·2	3·5	2·7	5·1	8·5	3·4	5·1	7·5	5·0	5·3	3·8	1·6
Cr	136	90	114	278	295	202	236	250	148	178	144	91
Co	150	143	144	139	150	153	139	145	162	172	180	180
Ni	3163	2892	3069	3050	3177	3275	2992	2817	3026	2125	2561	2869
Rb	0·08	<0·03	0·05	<0·37	0·12	0·03	0·03	0·09	0·27	<0·10	<0·63	0·01
Ba	<0·04	0·03	<0·01	<0·03	0·55	<0·35	<0·55	0·83	<0·50	<0·04	0·04	0·10
Sr	0·11	<0·01	<0·09	<0·01	<0·50	<0·02	1·36	0·65	0·22	<0·03	0·05	0·22
Pb	0·08	<0·09	0·10	0·14	0·08	0·15	0·30	0·24	0·10	0·21	0·17	0·12
Th	<0·01	<0·02	<0·02	<0·03	0·03	0·02	<0·01	0·04	<0·02	0·04	0·03	0·01
U	<0·01	<0·10	<0·05	0·01	0·03	0·03	0·05	<0·04	<0·02	0·02	0·01	0·01
Nb	<0·03	<0·13	<0·01	0·18	0·11	0·20	0·10	0·27	0·05	0·02	0·05	0·02
Ta	<0·04	<0·02	<0·01	0·01	<0·02	0·04	0·03	0·02	0·01	0·03	0·01	0·01
Ti	1·50	6·30	1·05	13·2	177	55·4	58·1	155	68·4	52·8	36·5	9·50
Zr	0·05	0·09	0·09	0·07	0·44	0·10	0·15	0·15	<0·25	0·27	<0·15	0·07
Hf	<0·12	<0·01	<0·01	0·02	0·05	<0·06	<0·13	0·02	<0·10	0·07	<0·06	0·03
La	<0·02	<0·04	0·03	<0·08	<0·09	<0·02	0·03	0·24	<0·02	0·03	0·03	0·04
Ce	<0·03	<0·05	0·02	<0·01	0·23	0·05	0·32	<0·70	<0·02	<0·01	0·03	0·03
Nd	<0·01	<0·06	<0·21	<0·41	0·10	<0·01	0·21	<0·47	<0·11	<0·13	<0·07	0·05
Sm	<0·01	<0·09	<0·14	<0·24	0·04	<0·10	<0·05	<0·07	<0·07	0·07	<0·08	<0·05
Eu	<0·03	<0·01	<0·03	<0·01	<0·03	<0·01	<0·06	<0·08	<0·03	0·02	<0·03	<0·05
Gd	<0·01	<0·09	<0·33	0·03	0·04	<0·06	0·02	<0·10	<0·10	<0·26	<0·08	0·05
Dy	<0·07	<0·18	<0·03	<0·23	<0·12	<0·18	<0·01	<0·01	<0·25	0·07	0·01	0·05
Ho	<0·03	<0·02	<0·04	<0·05	0·02	<0·04	0·01	<0·03	<0·02	<0·05	<0·03	0·01
Er	<0·08	<0·07	0·02	0·03	0·04	<0·06	0·02	<0·08	0·01	<0·08	0·01	0·03
Yb	<0·02	<0·15	<0·18	<0·03	<0·03	<0·02	0·02	<0·06	0·01	<0·17	0·02	0·03
Lu	<0·01	<0·01	<0·06	<0·01	<0·05	<0·02	0·01	<0·01	0·01	0·03	0·01	0·01
Y	0·01	<0·09	<0·01	<0·05	0·09	<0·14	0·39	<0·16	<0·02	<0·02	0·10	0·10

spinel from dunite typically have very low contents of incompatible trace elements, most below detection limits (Tables 5 and 6). Spinel displays a large range of Ti contents (Table 6). Some spinel grains may contain small amounts of Zr (0·50–4 ppm) and Nb (0·25–1 ppm). Ti content of olivine ranges from 9·50 to 68·35 ppm.

Incompatible trace elements in protogranular, clinopyroxene-bearing harzburgite

Incompatible trace element contents are commonly below detection limits for olivine, orthopyroxene and spinel (Tables 5–7). Bulk-rock samples and clinopyroxene grains of protogranular harzburgite display very uniform heavy REE (HREE) contents. Lu_{cpx} and $Lu_{bulk\ rock}$ range from 0·5 to 1·5 and from 0·03 to 0·08 times the primitive mantle value, respectively. Sample OB-93-67b shows the lowest La and Ce contents and the highest Yb and Lu contents, but all samples are richer in LREE than in middle REE (MREE) (Fig. 2). Sample OB-93-426 displays the highest REE contents, in both clinopyroxene and the bulk rock. Clinopyroxene from protogranular harzburgite samples has pronounced depletion in Ba, Zr and Ti, and enrichment in U and Pb (Fig. 2). Two other

Table 6: Representative spinel trace element analyses (LA-ICP-MS) from type I mantle xenoliths from the Kerguelen Islands (values in ppm)

Sample:	OB-93-58	OB-93-279	OB-93-426	OB-93-22	GM-92-501	OB-93-3	OB-93-5	JGM-92-1c	GM-92-480	BOB-93-640.1	MM-94-101	MG-91-143
n:	2	2	2	2	2	2	2	2	2	2	2	2
Sc	3·6	3·1	3·1	2·3	3·3	3·5	3·4	2·8	3·1	2·8	5·6	1·8
V	1025	1039	898	670	834	420	490	890	887	979	1005	550
Co	272	258	278	187	193	258	202	232	271	286	316	293
Ni	1644	1343	1332	1667	2542	2310	2502	2762	2366	1255	2594	1219
Rb	2·40	5·04	2·14	0·82	0·94	0·63	<0·07	1·60	0·62	1·39	0·28	n.d.
Ba	0·06	0·96	0·24	<0·16	0·13	<0·01	<0·02	<0·50	<0·03	0·01	0·57	n.d.
Sr	0·24	0·77	0·36	0·14	0·06	0·99	2·04	1·13	1·88	0·16	2·77	2·64
Pb	0·44	0·33	0·32	<0·12	0·05	<0·07	0·50	0·10	<0·05	0·51	0·60	0·36
Th	0·01	<0·01	0·03	0·04	0·02	<0·02	<0·07	0·02	0·03	0·03	0·04	<0·04
U	<0·01	<0·03	<0·07	<0·01	0·07	<0·07	0·06	<0·02	0·01	<0·05	0·01	0·09
Nb	0·70	0·54	0·71	1·13	0·65	0·54	0·38	0·67	0·69	0·28	0·71	2·29
Ta	<0·02	<0·01	<0·05	0·08	0·22	<0·01	<0·01	0·01	0·05	0·05	<0·01	0·06
Ti	115	183	360	1338	12906	3012	1700	10360	4843	5771	6655	2435
Zr	0·48	1·08	0·68	2·00	1·12	1·60	0·65	1·00	0·50	1·17	1·10	2·28
Hf	<0·02	<0·01	<0·40	<0·03	0·05	<0·09	0·01	0·08	0·10	0·23	<0·15	0·05
La	<0·01	<0·04	<0·03	<0·02	0·08	0·07	0·16	0·04	<0·03	<0·02	0·18	0·03
Ce	<0·01	0·05	0·07	<0·01	0·66	0·27	0·43	0·01	<0·40	0·02	0·39	<0·15
Nd	<0·11	<0·25	<0·50	<0·32	0·15	<0·60	0·39	<0·10	<0·20	<0·25	0·07	0·06
Sm	<0·07	<0·01	<0·02	<0·13	0·01	<0·12	<0·10	<0·03	<0·18	0·14	0·01	<0·20
Eu	<0·04	<0·06	0·02	<0·07	<0·02	<0·03	0·12	<0·04	<0·05	0·06	<0·01	0·05
Gd	<0·02	<0·10	<0·03	<0·20	0·19	<0·18	<0·13	<0·12	<0·01	<0·04	<0·34	0·04
Dy	<0·08	<0·07	<0·13	<0·15	<0·04	<0·20	0·18	<0·01	<0·15	<0·25	<0·05	0·05
Ho	<0·02	<0·06	<0·02	<0·12	0·03	<0·04	<0·06	<0·03	<0·03	<0·10	0·05	<0·01
Er	<0·04	<0·16	<0·14	<0·07	0·13	<0·01	0·12	<0·02	<0·20	<0·03	<0·08	0·06
Yb	<0·01	<0·03	<0·30	<0·06	0·03	<0·11	0·17	0·11	0·04	<0·11	0·04	<0·10
Lu	<0·01	<0·03	<0·05	<0·04	0·02	<0·02	0·02	0·01	<0·07	0·03	0·08	0·03
Y	0·03	0·11	0·10	<0·03	0·02	<0·11	<0·03	0·01	<0·15	<0·09	<0·01	0·02

n.d., not determined.

LREE-rich clinopyroxenes (samples OB-93-426 and OB-93-58) also show a significant depletion in Nb. Samples OB-93-426, BOB-93-666, OB-93-67b and OB-93-279 show a depletion in Sr. Bulk-rock trace element patterns display high enrichment in Pb and Sr and commonly an enrichment in Ti (Fig. 2). Sample BOB-93-666 has high Rb and Ba contents. Orthopyroxene from protogranular harzburgite samples shows significant amounts of Ti and around 1 ppm of Ga (Table 7). Other incompatible trace element contents of orthopyroxene are very low but the LREE content of orthopyroxene from sample OB-93-426 is higher than that of orthopyroxene from the other protogranular harzburgite samples (Table 7). Olivine has low Ti contents and very low Zr and Pb contents (Table 5). Spinel from sample OB-93-426 contains more Ti than those from the four other protogranular harzburgite samples (Table 6). Spinel from protogranular harzburgite samples also has low Rb, Sr, Zr, Nb and Pb contents (Table 6).

Incompatible trace elements in poikilitic clinopyroxene-bearing harzburgites and clinopyroxene-poor lherzolite

Incompatible trace element (ITE) contents of poikilitic peridotites and their constituent minerals are much higher than those of protogranular samples (Tables 4–8, Figs 2 and 3). Olivine from poikilitic peridotite samples contains low amounts of Ti, Zr and Pb (Table 5). Spinel grains

Table 7: Representative orthopyroxene trace element analyses (LA-ICP-MS) from type I mantle xenoliths from the Kerguelen Islands (values in ppm)

Sample:	OB-93-58	OB-93-279	OB-93-426	OB-93-22	GM-92-501	OB-93-3	OB-93-5	JGM-92-1c
n:	3	3	3	3	3	3	3	3
Sc	22·1	28·0	21·2	18·1	16·2	15·5	17·4	15·0
V	74·1	131·3	70·0	75·0	104·5	70·0	77·5	96·1
Cr	3438	3620	4051	4050	4985	3690	3083	3910
Co	57·9	56·3	55·1	60·6	64·4	61·5	53·1	64·2
Ni	786	689	753	912	895	815	708	788
Rb	<0·39	0·11	0·15	0·12	0·28	0·22	0·08	0·10
Ba	<0·05	0·08	0·11	0·05	0·46	0·60	0·05	0·16
Sr	0·10	0·14	<0·12	2·04	1·54	1·90	2·14	1·15
Pb	<0·19	0·04	0·04	0·14	0·45	0·15	0·31	0·20
Th	<0·03	0·04	<0·04	0·04	0·02	0·02	0·05	0·03
U	<0·03	<0·02	0·01	0·06	0·03	0·03	0·02	0·01
Nb	0·08	<0·04	0·04	0·14	0·13	0·14	0·12	0·11
Ta	<0·03	<0·01	0·04	0·02	<0·05	<0·06	0·03	0·05
Ti	24·5	31·2	104	220	1626	44·0	786	2548
Zr	0·20	0·24	0·10	6·50	4·35	6·50	3·01	8·10
Hf	<0·11	0·01	0·02	0·08	0·15	0·28	0·11	0·35
La	<0·03	<0·05	0·03	0·07	0·09	0·14	0·14	0·08
Ce	<0·04	0·03	0·15	0·16	0·24	0·44	0·38	0·25
Nd	<0·15	<0·07	0·22	0·14	0·24	0·45	0·33	0·32
Sm	<0·09	<0·02	0·06	0·07	0·12	0·18	0·14	<0·15
Eu	<0·04	<0·02	0·02	0·03	0·04	0·08	0·06	0·05
Gd	<0·12	<0·02	0·06	<0·25	0·20	0·30	0·20	0·28
Dy	<0·12	<0·05	0·05	0·15	0·28	0·37	0·25	0·35
Ho	<0·04	<0·04	<0·01	0·04	0·07	0·09	0·04	0·09
Er	<0·02	<0·03	<0·11	<0·22	0·23	0·33	0·16	0·28
Yb	<0·08	0·02	0·06	0·14	0·30	0·43	0·18	0·35
Lu	0·01	<0·02	0·02	0·02	0·05	0·07	0·03	0·06
Y	<0·07	0·07	0·11	0·50	1·07	1·50	1·25	1·60

of poikilitic peridotite samples are richer in Ti than those of protogranular harzburgite samples. They contain low amounts of Rb, Sr, Zr and Nb (Table 6). The poikilitic, clinopyroxene-poor lherzolite contains clinopyroxene and orthopyroxene richer in Ti than those of poikilitic harzburgite samples (Tables 7 and 8).

REE compositions of both bulk rock and minerals are very uniform (Figs 3 and 5). Clinopyroxene is poor in Ba, Nb, Pb, Sr, Zr and Ti (Fig. 3).The bulk rocks are uniformly poor in Ba but not in Nb, Pb, Sr, Zr and Ti (Fig. 3). For example, the anhydrous sample GM-92-501 shows no depletion in Nb and Pb, depletion in Sr and Zr, and enrichment in Ti (Fig. 3). On the other hand, the amphibole + phlogopite-bearing sample OB-93-5 displays no depletion in Nb and Sr but it is depleted in Pb, Zr and Ti (see Fig. 3 for other samples). Orthopyroxene grains have lower REE contents than primitive upper mantle and display LREE-depleted REE patterns (Fig. 3). They are also relatively poor in Ba, Sr and Pb but rich in Zr and Ti. However, orthopyroxene from samples OB-93-3 and OB-93-22 is poor in Ti, and that from sample OB-93-5 is poor in Zr (Fig. 3). Phlogopite from samples OB-93-5 and OB-93-3 displays REE contents lower than those of the primitive mantle (Fig. 5 and Table 9). The phlogopite grains are rich in Rb, Ba, Nb and Ta, and contain significant amounts of Sr, Ti, Pb, Zr and Hf, but are poor in Th, U and Y (Table 9). Amphibole from sample OB-93-5 displays high ITE contents and LREE-enriched patterns, but is poor in U, Ta, Pb, Zr and Hf (Fig. 5).

Table 8: Representative clinopyroxene trace element analyses (LA-ICP-MS) from type I mantle xenoliths from the Kerguelen Islands (values in ppm)

Sample:	OB-93-58	OB-93-279	OB-93-426	OB-93-22	GM-92-501	OB-93-3	OB-93-5	JGM-92-1c	GM-92-480	BOB-93-640.1	MM-94-101	MG-91-143
n:	4	4	4	4	4	4	4	4	4	4	4	4
Sc	53	60	62	62	54	73	67	45	89	128	129	93
V	176	217	139	160	241	212	225	241	255	182	310	202·5
Co	33·0	19·0	18·6	19·9	26·7	23·8	17·6	21·6	19·3	31·6	23·1	22·3
Ni	489	326	313	374	418	400	277	340	288	286	272	286
Rb	0·22	0·95	0·36	0·05	0·34	0·08	0·06	n.d.	0·87	1·22	0·35	0·12
Ba	0·29	0·07	0·10	0·26	0·68	0·29	0·05	n.d.	2·75	2·77	2·74	1·18
Sr	1·20	0·72	6·00	282	203	292	371	221·1	230·3	208·5	134	458
Pb	0·36	0·34	0·33	0·16	0·50	0·19	0·34	0·45	0·59	0·79	0·22	2·96
Th	0·06	0·02	0·05	0·56	0·70	0·13	0·46	1·17	0·21	0·59	1·22	2·61
U	0·03	0·03	0·02	0·08	0·08	0·04	0·08	0·26	0·03	0·16	0·23	1·12
Nb	0·22	0·25	0·35	2·28	0·65	1·47	1·34	2·01	1·34	0·85	0·97	0·77
Ta	<0·05	<0·06	<0·05	0·44	0·07	0·28	0·19	0·20	0·33	0·14	0·09	0·02
Ti	61	60	205	530	4080	2100	3480	8510	3730	2770	4070	827
Zr	0·30	0·74	2·20	62·0	50·5	300	118	118	190	59·1	225	53·9
Hf	<0·05	<0·10	<0·12	1·06	1·35	7·92	3·49	5·50	4·55	1·38	5·54	1·03
La	0·85	0·34	1·20	18·3	8·7	17·8	28·6	14·3	8·8	11·4	14·2	62·0
Ce	1·00	0·75	0·71	34·0	20·3	65·4	81·9	38·0	29·3	23·6	34·0	151
Pr	0·11	0·09	0·25	4·20	2·79	11·3	11·2	5·80	4·90	2·97	4·54	n.d.
Nd	0·47	0·37	0·96	12·5	14·6	58	54	30	25	12·9	21	67
Sm	0·10	0·07	0·26	1·7	3·2	12·8	9·9	8·0	6·3	2·2	4·9	12·0
Eu	0·03	0·02	0·09	0·45	1·04	4·0	2·9	2·6	2·0	0·76	1·6	3·9
Gd	0·10	0·09	0·28	1·44	3·4	12·0	8·1	8·5	5·9	2·30	5·60	8·76
Tb	0·02	0·02	0·05	0·17	0·43	1·58	1·16	1·24	0·85	0·33	0·78	n.d.
Dy	0·11	0·13	0·36	0·70	2·7	8·9	6·2	6·8	4·6	1·80	4·98	6·54
Ho	<0·02	0·04	0·08	0·08	0·47	1·60	1·00	1·25	0·82	0·38	1·05	1·19
Er	0·10	0·16	0·27	0·32	1·05	3·94	2·43	2·96	2·01	1·09	2·55	2·86
Yb	0·23	0·32	0·40	0·23	0·86	2·65	1·81	2·16	1·51	1·02	1·93	2·59
Lu	0·07	0·10	0·09	0·06	0·10	0·34	0·24	0·30	0·20	0·16	0·26	0·38
Y	0·23	0·53	1·90	4·00	12·0	36·5	26·7	27·5	19·0	10·5	24·9	31·1

n.d., not determined.

Incompatible trace elements in clinopyroxene + phlogopite-bearing dunites

Phlogopite-bearing, amphibole-free dunite samples have uniform REE and trace element bulk-rock contents. They display LREE-rich or upward convex REE patterns, and are rich in Ti and Pb, and poor in Zr (Fig. 4). Sample MM-94-54 is rich in Th, U and Sr. Sample GM-92-480 is rich in Sr, Rb, Ba, Nb and Ta (Fig. 4). Clinopyroxene grains in this suite display LREE-rich or upward convex REE patterns, are poor in Pb and Ti, but otherwise have incompatible trace element patterns similar to those of clinopyroxene from the poikilitic harzburgite (Fig. 4). Samples BOB-93-640.1, MM-94-54, MM-94-97 and MM-94-101 contain clinopyroxene that is poor in Nb and Zr and of variable Sr contents. Clinopyroxene from sample GM-92-480 is poor in the most incompatible elements (Rb, Ba, Th, U and Nb) and in Zr (Fig. 4). Clinopyroxene from sample GM-92-468 is the richest in moderately incompatible trace elements (from Sr to Lu, Fig. 4). It is also rich in Hf and poor in Sr. Phlogopite grains from this suite resemble counterparts from poikilitic harzburgite (Fig. 5). Both are rich in Rb, Ba, Nb, and Ta, and poor in Th, U and REE (Table 9, Fig. 5).

Table 9: Representative phlogopite and amphibole trace element analyses (LA-ICP-MS) from type I mantle xenoliths from the Kerguelen Islands (values in ppm)

	Phlogopite					Amphibole	
Sample:	OB-93-3	OB-93-5	GM-92-480	MM-94-101	MG-91-143	OB-93-5	MG-91-143
n:	4	4	4	3	4	5	3
Sc	5·5	8·5	8·0	10·3	3·3	47	52
V	240	360	279	350	135	340	256
Co	63	69	53	68	66	31	48
Ni	1750	1735	1334	1434	1440	687	812
Rb	382	331	174	200	416	6·55	6·00
Ba	2160	2560	1715	1273	1361	111	43
Sr	249	367	202	161	147	852	687
Pb	0·65	2·02	0·88	0·90	5·8	1·02	7·58
Th	0·04	0·11	0·07	0·12	0·06	1·14	3·77
U	0·02	0·05	0·02	0·04	0·26	0·08	1·98
Nb	92	69	65	98	38	33	63
Ta	6·2	3·1	5·1	5·9	1·4	1·00	1·39
Ti	27500	25700	24360	31450	8220	16900	7300
Zr	49	33	40	65	8·2	107	100
Hf	0·90	0·26	0·70	1·28	0·18	1·56	1·49
La	0·29	0·15	0·07	0·04	0·21	39	83
Ce	0·83	0·35	0·21	0·25	0·48	83	191
Nd	0·55	0·49	0·14	0·25	0·35	36	80
Sm	0·20	0·15	0·07	0·11	0·12	6·2	13·8
Eu	0·10	0·10	0·03	0·05	0·04	2·1	4·5
Gd	0·38	0·23	<0·25	<0·32	0·12	4·9	9·7
Dy	0·32	<0·25	<0·30	0·25	0·15	4·1	6·9
Ho	0·08	0·05	0·06	0·06	0·04	0·60	1·2
Er	0·22	0·13	<0·25	<0·30	0·11	2·1	2·9
Yb	0·25	0·15	0·20	0·13	0·10	1·2	2·4
Lu	0·04	0·03	0·03	0·02	0·02	0·18	0·32
Y	1·05	0·89	0·11	0·08	0·12	18·7	31·8

Clinopyroxene and amphibole from amphibole- and phlogopite-bearing dunite sample MG-91-143 display similar REE contents and LREE-rich REE patterns (Figs 4 and 5). Clinopyroxene is poorer in Rb, Ba, Nb, Ta, Ti, Zr and Hf than amphibole. Phlogopite grains (Fig. 5) contain less Ti, Nb, Ta, Zr and Hf, and more Rb, Pb and U than those found in amphibole-free dunite and poikilitic harzburgite samples.

Origin and evolution of Kerguelen mantle xenoliths

Partial melting characteristics

Both types of clinopyroxene-bearing harzburgites and the clinopyroxene-poor lherzolite display features of residues of high degrees of partial melting. Bulk-rock compositions rich in MgO, Ni and Co and poor in CaO, Al_2O_3, Na_2O, Sc and V result from the preferential melting of clinopyroxene and spinel and retention of olivine and orthopyroxene (Mysen & Kushiro, 1977; Presnall *et al.*, 1978; Kostopoulos, 1991). The high *mg*-numbers of the bulk rocks, olivine and pyroxenes, along with low and uniform HREE content, imply that a significant amount of basaltic melt was removed from protogranular harzburgites. Fifteen to 25 wt % melting of Kerguelen protogranular harzburgite was estimated by Grégoire *et al.* (1997). This result is consistent with the presence of clinopyroxene in even the most depleted protogranular harzburgites (Elthon, 1993). Kerguelen mantle xenoliths lack the LREE-depleted patterns of

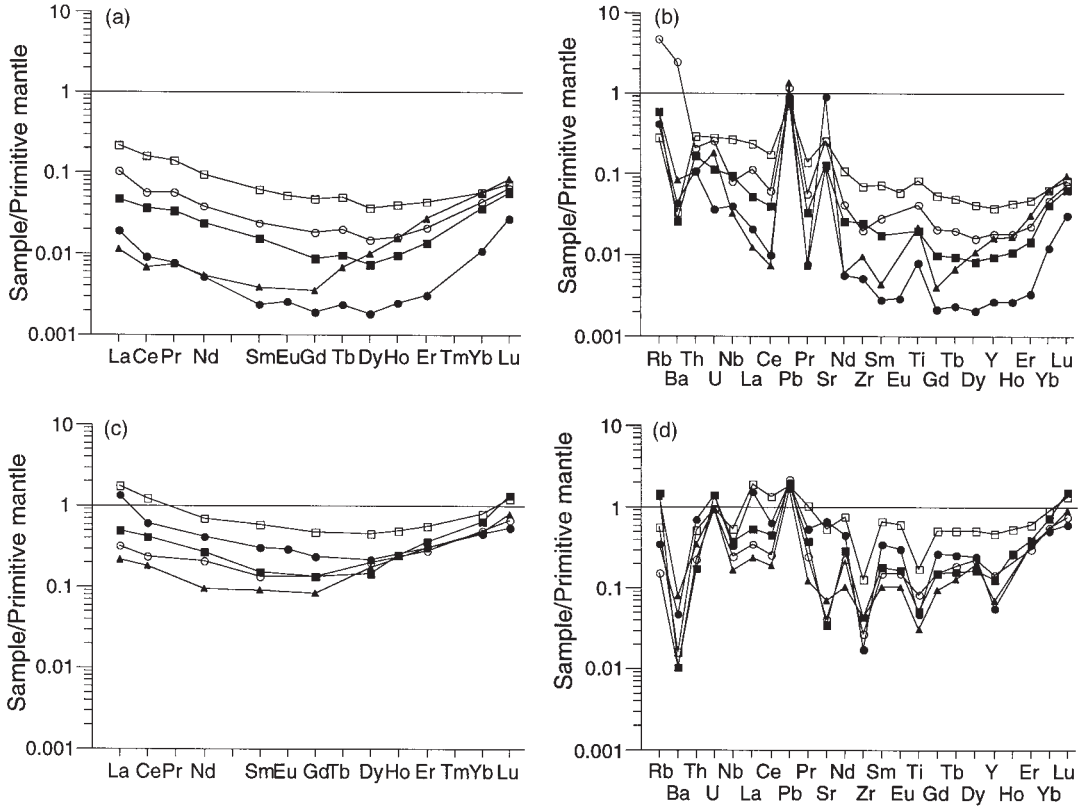

Fig. 2. Primitive mantle-normalized REE and incompatible trace element patterns for whole rock (a,b) and clinopyroxene (c,d) from Kerguelen protogranular harzburgite samples. Normalizing values after McDonough & Sun (1995). ○, sample BOB-93-666; ● sample OB-93-58; □, sample OB-93-426; ■, sample OB-93-279; ▲, sample OB-93-67b. In primitive mantle-normalized trace element plots, the sequence of elements is related to their decreasing incompatibility during partial melting of upper-mantle peridotites (Sun & McDonough, 1989).

mantle peridotites from oceanic settings (e.g. abyssal peridotites, Johnson *et al.*, 1990; Hawaiian peridotites, Sen *et al.*, 1993; Yang *et al.*, 1998) that result from a simple residue model.

Metasomatic characteristics

The consistent enrichment of highly incompatible trace elements in the harzburgites and clinopyroxene-poor lherzolite requires metasomatic reactions [see also Hassler & Shimizu (1998)]. In addition to incompatible trace element enrichment, poikilitic peridotite samples display lower bulk-rock and mineral *mg*-numbers than those of protogranular harzburgite, and contain Na-, Cr-, Al- and Ti-rich magnesian augite, ± phlogopite and amphibole. U-shaped patterns similar to those of protogranular harzburgite samples are found in metasomatized refractory mantle spinel peridotites, both as xenoliths entrained in alkali basalts (Downes & Dupuy, 1987; Siena *et al.*, 1991; Xu *et al.*, 1998) and in orogenic lherzolite massifs (Bodinier *et al.*, 1991; Downes *et al.*, 1991). The LREE-enriched or upward convex REE patterns of both bulk-rock samples and clinopyroxene from the poikilitic harzburgite closely resemble those of alkaline cumulate rocks and peridotite infiltrated by alkaline silicate melts (Bodinier *et al.*, 1988; Fabriès *et al.*, 1989; Xu *et al.*, 1998). The difference between the two types of REE patterns can be explained by a chromatographic effect (Navon & Stolper, 1987; Bodinier *et al.*, 1988).

The presence of phlogopite ± amphibole and the major and trace element compositions of minerals and bulk rocks preclude an origin for Kerguelen dunite as single residues of partial melting processes [see also Grégoire *et al.* (1997)]. Furthermore, minerals in most of phlogopite-bearing dunite samples display incompatible trace element characteristics similar to those of poikilitic Mg-augite-bearing harzburgite (except for the phlogopite + amphibole-bearing dunite sample).

To assess the nature of the metasomatic agents we calculated melt compositions in equilibrium with clinopyroxene in poikilitic harzburgite, clinopyroxene-poor lherzolite and dunite. We used two sets of clinopyroxene–melt partition coefficients to assess the possible effect of the range of these values on the results. The first set is average $D_{cpx/sil} = D_{clinopyroxene/mafic\ silicate\ melts}$, with most

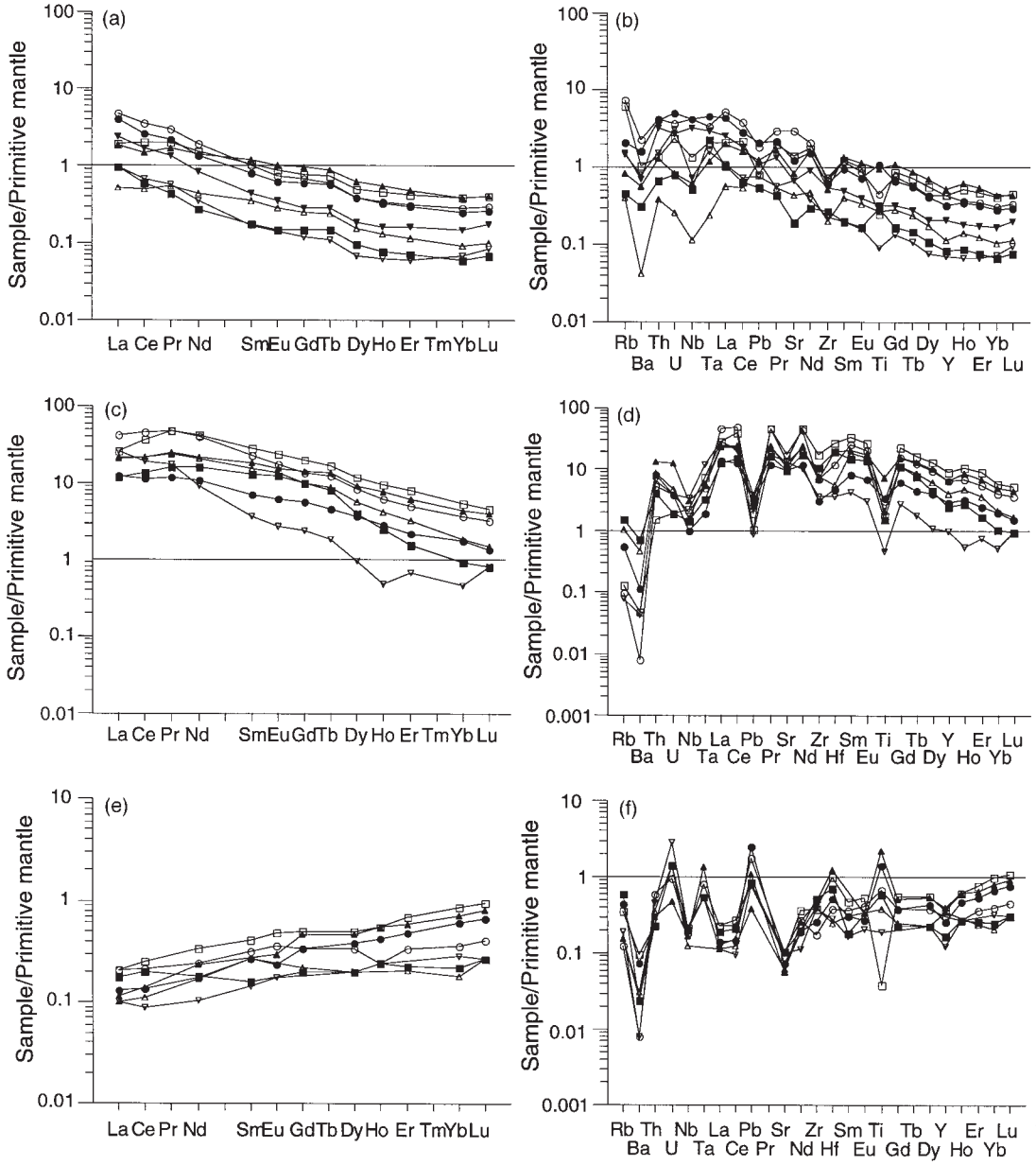

Fig. 3. Primitive mantle-normalized REE and incompatible trace element patterns for whole rock (a,b), clinopyroxene (c,d) and orthopyroxene (e,f) from Kerguelen poikilitic harzburgites and clinopyroxene-poor lherzolite. Normalizing values after McDonough & Sun (1995). ○, sample OB-93-5; ●, sample GM-92-501; □ , sample OB-93-3; ■, sample GM-92-502; ▲, sample JGM-92-lc (cpx-poor lherzolite); △, sample GM-92-453; ▽, sample MG-91-260.

elements from the compilation of Chazot *et al.* (1996), the value for Ti from Hart & Dunn (1993) and the value for Ta from Chalot-Prat & Boullier (1997). The other set of coefficients is $D_{cpx/carb} = D_{clinopyroxene/carbonatitic\ melts}$, with most elements from Klemme *et al.* (1995), except for the value for Rb, from Green *et al.* (1992).

Melts display trace element contents 10–5000 times those of the primitive mantle (except for Ti, Ta and Zr calculated with $D_{cpx/carb}$; Fig. 6). The two calculated melt compositions for amphibole + phlogopite-bearing dunite sample MG-91-143 are similar. Both are depleted in Nb, Ta, Zr, Hf and Ti (Figs 6 and 7; see Hauri *et al.*, 1993; Chazot *et al.*, 1994; Baker *et al.*, 1998).

Model melt compositions for poikilitic harzburgite, clinopyroxene-poor lherzolite and phlogopite-, clinopyroxene-bearing dunite suggest that all these rocks could

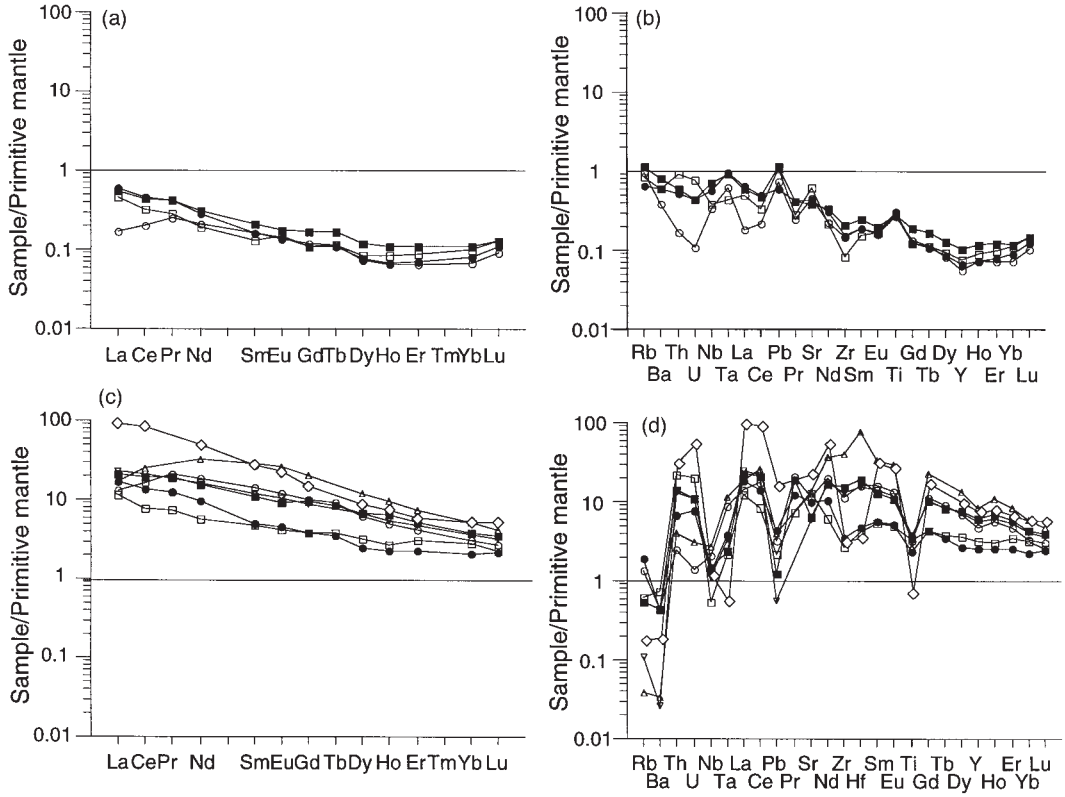

Fig. 4. Primitive mantle-normalized REE and incompatible trace element patterns for whole rock (a,b) and clinopyroxene (c,d) from Kerguelen Clinopyroxene + phlogopite ± amphibole-bearing dunites. Normalizing values after McDonough & Sun (1995). ○, sample GM 92-480; ●, sample BOB-93-640·1; □, sample MM-94-54; ■, sample MM-94-101; △, sample GM-92-468; ▽, sample MM-94-97; ◇, sample MG-91-143 (phlogopite + amphibole sample).

have been in equilibrium with a CO_2-rich silicate melt (Figs 6 and 7). However, the high field strength element (HFSE) contents of the model melt depend on the partition coefficient dataset. Using the $D_{cpx/carb}$ we obtained an equilibrium melt poor in HFSE, but not as HFSE poor as melt in equilibrium with sample MG-91-143 (Fig. 7). However, $D_{cpx/sil}$ values yield model melts that are relatively undepleted in Nb, Zr and Hf, and only slightly depleted in Ti. The calculated equilibrium melt for $D_{cpx/sil}$ resembles that of ultramafic and alkaline lamprophyre in its incompatible trace element composition but not that of carbonatites (Fig. 7). The equilibrium melts calculated with $D_{cpx/carb}$ have geochemical signatures consistent with either carbonatite or ultramafic and alkaline lamprophyre (Fig. 7).

In summary, the amphibole + phlogopite dunite (MG-91-143) probably was metasomatized by a CO_2-rich silicate melt. The poikilitic harzburgite, clinopyroxene-poor lherzolite and phlogopite-bearing dunite samples probably were metasomatized by highly alkaline mafic silicate melts. Such magmas have been already described from oceanic settings (Yagi *et al.*, 1975; Nixon *et al.*, 1980; Rock, 1987), and young dykes with 'lamprophyric affinities' are found in the Kerguelen Islands (Leyrit, 1992; Moine, 2000).

Mantle history of the Kerguelen xenoliths

The origin and evolution of the two types of Kerguelen clinopyroxene-bearing harzburgites and clinopyroxene-poor lherzolite can be summarized in two main steps, namely, early partial melting (15–25%, Grégoire *et al.*, 1997) followed by metasomatism as a result of percolation of highly alkaline silicate melts into the previously depleted upper mantle. The metasomatism is cryptic in protogranular harzburgite and probably related to the percolation of a small volume of melt into the protogranular harzburgite, because it is manifested only in a slight enrichment in the most incompatible trace elements. The metasomatism is modal in poikilitic harzburgite and clinopyroxene-poor lherzolite, because incompatible trace enrichment is accompanied by crystallization of Mg-augite ± phlogopite ± amphibole. Some harzburgite samples display evidence of a later discrete metasomatic event evidenced by the crystallization of feldspar + olivine + rutile + ilmenite + armalcolite + chromite paragenesis.

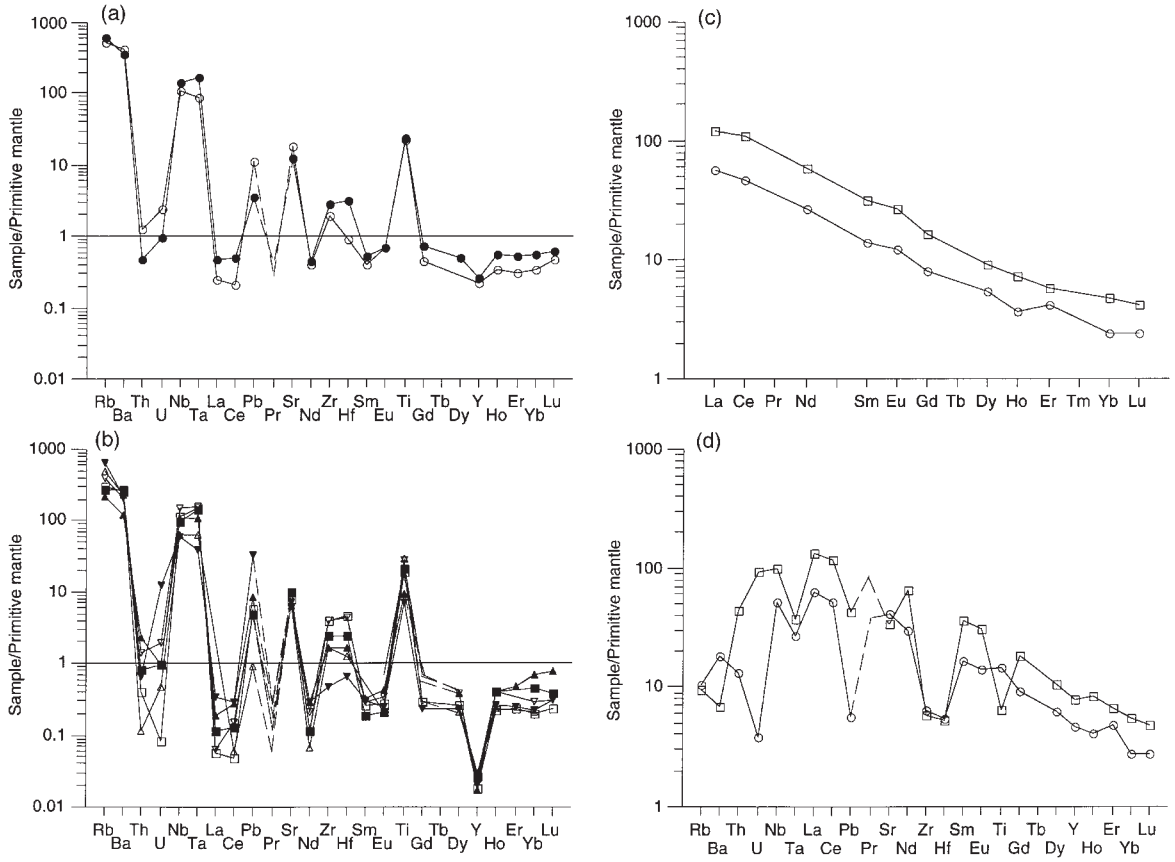

Fig. 5. Primitive mantle-normalized incompatible trace element patterns for phlogopite from Kerguelen poikilitic harzburgite samples OB-93-5 and OB-93-3 (a) and clinopyroxene + phlogopite ± amphibole-bearing dunite (b), and primitive mantle-normalized REE (c) and incompatible trace element patterns (d) for amphibole from Kerguelen poikilitic harzburgite sample OB-93-5 and clinopyroxene + phlogopite + amphibole-bearing dunite sample MG-91-143. Normalizing values after McDonough & Sun (1995). Phlogopite and amphibole of harzburgite: ○, OB-93-5; ●, OB-93-3, Phlogopite of dunite: □, GM-92-468; ■, GM-92-480; ▲, MM-94-54; △, MM-94-97; ▽, MM-94-101; ▼, MG-91-143 phlogopite + amphibole sample. Amphibole of dunite: □, MG-91-143.

The origin of clinopyroxene + phlogopite ± amphibole-bearing dunite is not clear. The dunite may represent a high-pressure cumulate of basaltic magma, as has been suggested for Hawaiian dunites (Sen, 1987; Clague, 1988), which was later metasomatized by highly alkaline silicate melts or carbonate-rich melts. Alternatively, anhydrous dunite may have formed by a reaction between harzburgites and basaltic melts that led to the dissolution of orthopyroxene and crystallization of olivine (Grégoire *et al.*, 1997), and then been metasomatized by highly alkaline silicate melts or carbonate-rich melts that produced clinopyroxene + phlogopite or clinopyroxene + phlogopite + amphibole.

We favour the second hypothesis because: (1) the studied dunites display Ni, Sc and V contents similar to those of harzburgites; (2) in composite xenoliths, dunite hosts magmatic veins that show affinities with the tholeiitic–transitional and alkaline magmatic series from the Kerguelen archipelago (Grégoire, 1994; Grégoire *et al.*, 1997); (3) not all Kerguelen dunite is similar to Type II Kerguelen xenoliths (peridotites, pyroxenites and metagabbros), which are high-pressure cumulates from the tholeiitic–transitional and alkaline magmatic series of the archipelago (Grégoire, 1994; Grégoire *et al.*, 1997, 1998).

The reaction of mantle harzburgite with basaltic melts to form dunite, together with a large volume of basaltic intrusions at the crust–mantle boundary, may explain the very low MgO contents (typically 4–5%) of Kerguelen basalts that lack primary mantle-melt compositions (Gautier *et al.*, 1990; Weis & Frey, 1996; Grégoire *et al.*, 1998; Yang *et al.*, 1998).

Trace element partition coefficients

Mineral-pair partition coefficients

Our comprehensive set of trace element data for mantle peridotites allows us to determine partition coefficients

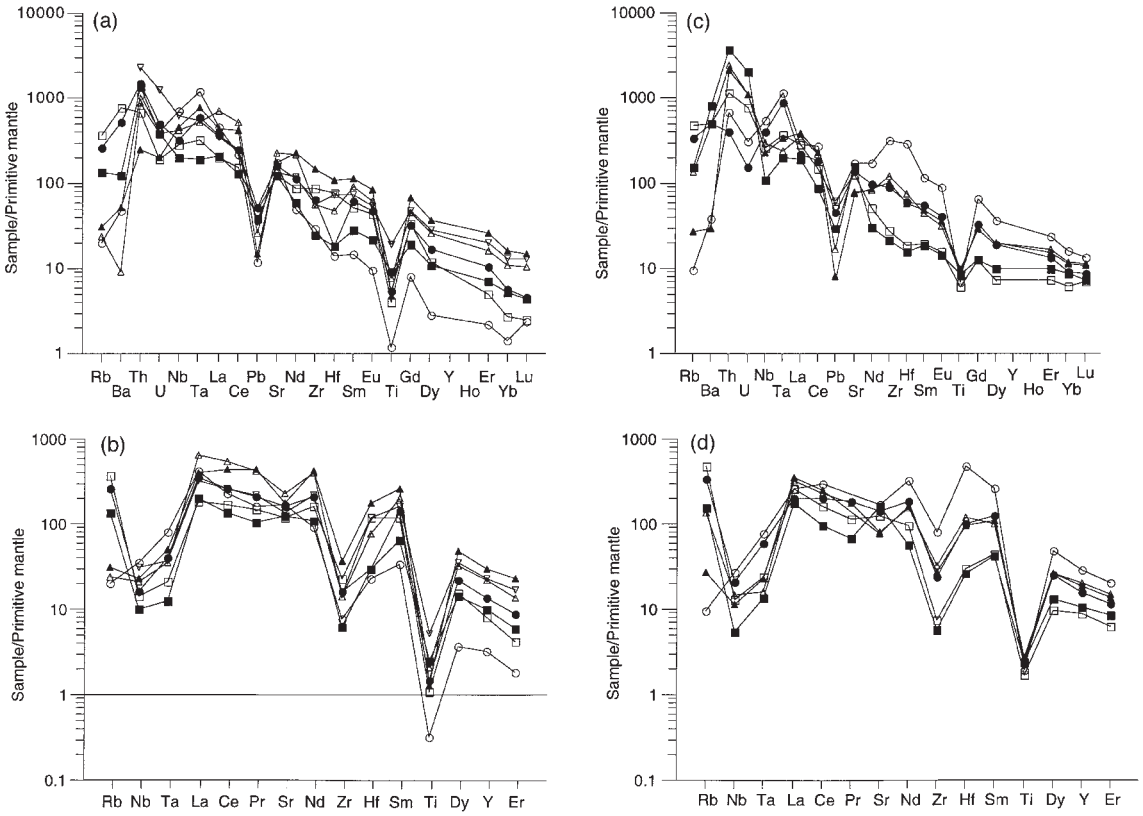

Fig. 6. Primitive mantle-normalized incompatible trace element patterns for liquid in equilibrium with clinopyroxene from Kerguelen poikilitic harzburgite cpx-poor lherzolite (a,b) and clinopyroxene + phlogopite ± amphibole-bearing dunites (c,d). Normalizing values after McDonough & Sun (1995). Calculations for (a) and (c) use cpx–basic silicate melt partition coefficients, and calculations for (b) and (d) use cpx–carbonatitic melt partition coefficients (see text for references). (a,b) ○, OB-93-22; ●, GM-92-453; □, GM-92-502; ■, GM-92-501; △, OB-93-5; ▲, OB-93-3; ▽, JGM-92-1c. (c,d) ○, GM-92-468; ●, GM-92-480; □, BOB-93-640·1; ■, MM-94-54; △, MM-94-101; ▲, MM-94-97.

for a wide range of elements in mantle clinopyroxene, orthopyroxene, olivine, spinel, amphibole and phlogopite. To establish meaningful intermineral partition coefficients, chemical equilibrium is required. The protogranular, clinopyroxene-bearing harzburgite samples display *mg*-number in olivine < *mg*-number in orthopyroxene < *mg*-number in clinopyroxene, as do numerous Type I mantle peridotites that represent equilibrium phase assemblages (e.g. Frey & Prinz, 1978; Brown *et al.*, 1980; Grégoire, 1994). The protogranular harzburgite samples are cryptically metasomatized but their mineral compositions do not vary within or between grains (Grégoire, 1994; Grégoire *et al.*, 1997). This indicates major element equilibration. We therefore assumed trace element equilibration and calculated two-mineral partition coefficients for ol–opx, ol–cpx, opx–cpx, sp–ol, sp–opx and sp–cpx in these rocks.

Poikilitic cpx-bearing harzburgite, clinopyroxene-poor lherzolite and dunite were modally metasomatized. This is evidenced by: (1) the addition of clinopyroxene ± phlogopite ± amphibole; (2) reaction of orthopyroxene and spinel inclusions in poikilitic cpx; (3) the high Fe_2O_3 and TiO_2 contents of spinel; (4) the higher Na_2O, Al_2O_3, TiO_2 and incompatible trace element contents of orthopyroxenes relative to protogranular orthopyroxenes; (5) the low *mg*-number of olivine. In dunite sample MG-91-143, amphibole has replaced interstitial clinopyroxene in a reaction relationship. Therefore, we calculated mineral-partition coefficients only for mineral pairs that crystallized from the same metasomatic agent: phlogopite–clinopyroxene in harzburgite and phlogopite-bearing, amphibole-free dunite samples, and amphibole–clinopyroxene and amphibole–phlogopite in the poikilitic harzburgite sample OB-93-5.

Partition coefficients (*D*) for trace elements in orthopyroxene and clinopyroxene pairs from protogranular harzburgite are <1 (Table 10) except for Co (2·53) and Ni (1·99). Values for other REE are two or three times those for La and Ce (Table 10). The greatest *D* values for incompatible trace elements are for Rb, Ba, Ti and Zr (Table 10). Our *D* values are much larger than those of Eggins *et al.* (1998). However, many interelement

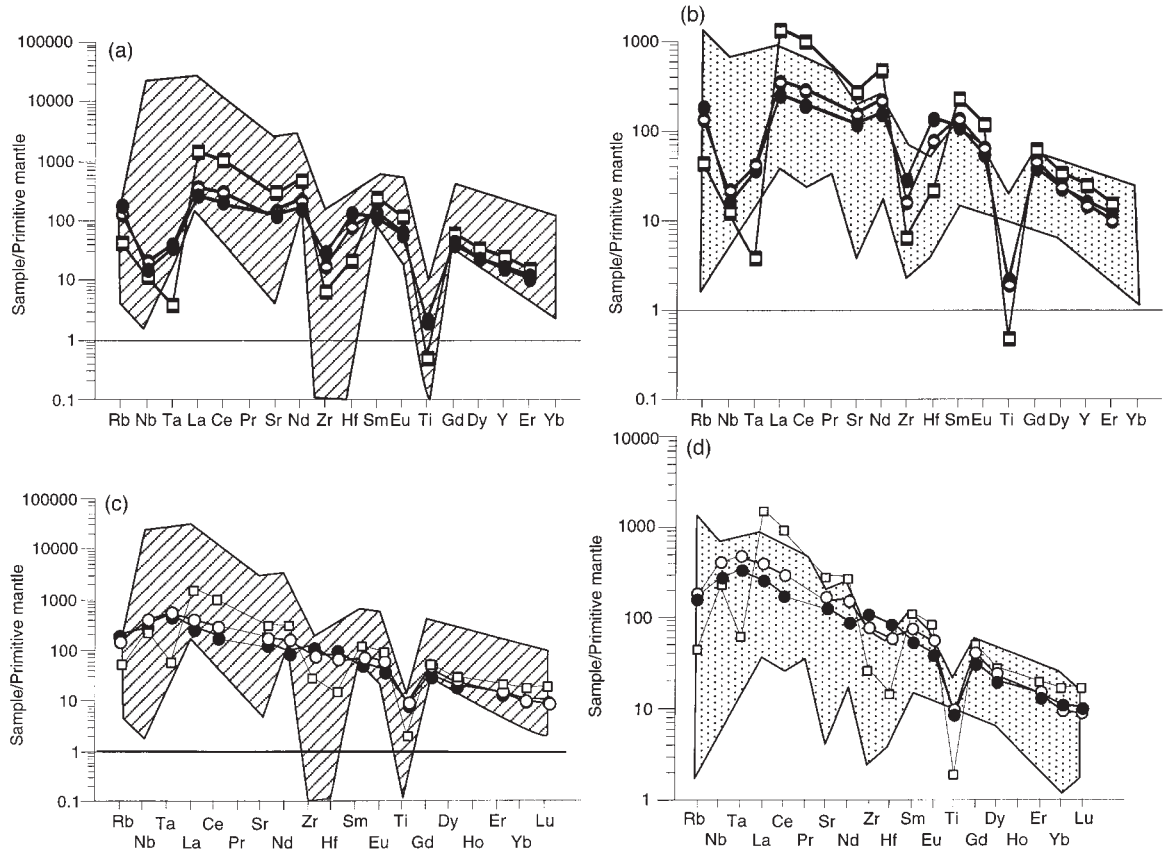

Fig. 7. Primitive mantle-normalized average compositions of incompatible trace element patterns for liquid in equilibrium with clinopyroxene from Kerguelen poikilitic harzburgites and cpx-poor lherzolite (○), clinopyroxene + phlogopite-bearing dunites (●) and clinopyroxene–phlogopite + amphibole-bearing dunite (MG-91-143, □). Normalizing values after McDonough & Sun (1995). Calculations use either cpx–carbonatitic melt partition coefficients (a,b) or cpx–basic silicate melt partition coefficient (c,d; see text for references). Dotted field, compositional field of ultramafic and mafic lamprophyres (Rock, 1987); hatched field, compositional field of carbonatites (Woolley & Kempe, 1989).

relationships are similar, e.g. D^{Ti} and $D^{Zr} > D^{REE}$. This may reflect a difference in the composition of clinopyroxene. In our samples, it is a Cr-diopside that is poor in incompatible trace elements, whereas Eggins *et al.* studied an Mg-rich augite that contains significant amounts of incompatible trace elements [compare Tables 2 and 8 of this study with table 1 of Eggins *et al.* (1998)]. Spinel strongly concentrates V and HFSE (Nb, Ta, Ti and Zr), and has $D_{sp/ol}$ and $D_{sp/opx}$ >1 for many trace elements (Table 10). Ni is partitioned preferentially into olivine but Co seems to be preferentially incorporated into spinel ($D_{sp/ol}$ = 1·92).

Partition coefficients between amphibole and clinopyroxene range from 0·45 to 3, except for Rb, Ba, Nb, Ta and Ti (Table 11 and Fig. 8a). Our results for Rb, Ba, Sr, Pb, U, Nb, Ti, Zr, La, Ce, Er, Yb and Lu agree with literature values, except that our *D* for Th is larger, and those of Hf and most REE (Nd to Ho) are smaller (Table 11 and Fig. 8a).

Average partition coefficients between phlogopite and clinopyroxene for poikilitic harzburgite, phlogopite-bearing dunite and amphibole + phlogopite-bearing dunite show that phlogopite strongly concentrates Ba, Rb, Nb, Ta, Co, Ni and Ti, and perhaps Pb, but incorporates lesser amounts of REE and Y, Zr and Hf relative to clinopyroxene (Table 11, Fig. 8b). Values of $D_{phl/cpx}$ for poikilitic harzburgite and phlogopite-bearing dunite resemble those found by Ionov *et al.* (1997).

Partition coefficients between phlogopite and amphibole indicate that phlogopite is enriched in Co, Ni, Rb, Ba, Pb, Nb, Ta and Ti relative to amphibole (Table 11). Other trace elements are preferentially incorporated into amphibole, except for V, which is equally partitioned between the two (Fig. 8c). Our results for Ti, Rb, Sr and Ba agree with those from the literature except that our D^{Zr} is slightly larger and our D^{Nb} is >1 (Table 11).

Table 10: Two-mineral partition coefficients for Kerguelen protogranular harzburgites

	opx/cpx		ol/opx		ol/cpx	
	average	range	average	range	average	range
Sc	0·40	0·34–0·47	0·14	0·12–0·20	0·06	0·05–0·07
V	0·51	0·42–0·60	0·04	0·02–0·04	0·02	0·015–0·020
Co	2·53	1·75–2·97	2·61	2·54–2·66	6·60	4·56–7·77
Ni	1·99	1·61–2·41	4·18	4·03–4·43	8·30	6·47–9·80
Rb	0·66	0·11–1·44	0·33	0·30–0·35	0·33	0·13–0·50
Ba	0·88	0·31–1·23	0·41	—	0·51	—
Sr	0·13	0·08–0·20	1·20	—	0·10	—
Pb	0·17	0·12–0·25	1·57	0·97–2·18	0·25	0·22–0·30
U	0·50	—	—	—	—	—
Th	—	—	2·40	—	1·00	—
Nb	0·20	0·11–0·36	—	—	—	—
Ti	0·50	0·40–0·58	0·08	0·01–0·20	0·04	0·005–0·10
Zr	0·40	0·14–0·67	0·50	0·25–0·95	0·16	0·12–0·20
Hf	0·14	0·08–0·20	—	—	—	—
La	0·02	—	1·16	—	0·03	—
Ce	0·05	0·04–0·07	0·13	—	0·01	—
Nd	0·23	—	—	—	—	—
Sm	0·22	—	—	—	—	—
Eu	0·23	—	—	—	—	—
Gd	0·21	—	—	—	—	—
Dy	0·14	—	—	—	—	—
Er	0·15	—	—	—	0·07	—
Yb	0·11	0·05–0·16	—	—	—	—
Lu	0·21	0·14–0·26	—	—	—	—
Y	0·09	0·07–0·14	—	—	0·03	—
	sp/opx		sp/cpx		sp/ol	
	average	range	average	range	average	range
Sc	0·18	0·14–0·22	0·07	0·05–0·10	1·37	0·73–1·83
V	12·50	11·60–13·84	6·34	5·82–7·09	363	325–443
Co	5·00	4·58–5·68	12·68	8·24–14·95	1·92	1·80–2·14
Ni	2·05	1·77–2·40	4·03	3·36–4·38	0·49	0·43–0·54
Rb	25·33	13·80–46·00	11·36	5·31–23·28	40·49	29·59–46·56
Ba	7·10	2·20–12·00	5·81	0·22–14·79	29·14	—
Sr	5·66	2·55–9·06	0·56	0·06–1·07	2·12	—
Pb	6·82	4·97–8·36	1·11	0·97–1·24	4·67	3·27–5·57
Th	—	—	0·38	0·14–0·63	—	—
Nb	16·87	8·74–23·20	2·56	2·02–3·18	—	—
Ta	—	—	4·92	—	—	—
Ti	4·37	3·45–5·87	2·18	1·76–3·05	136	28·95–342·14
Zr	4·42	2·38–6·80	1·48	0·96–1·90	9·57	7·17–12·04
Ce	1·05	0·47–1·62	0·08	0·03–0·16	3·53	—
Eu	1·16	—	0·26	—	—	—
Y	1·39	0·93–1·79	0·13	0·05–0·20	4·69	—

Ol, olivine; opx, orthopyroxene; cpx, clinopyroxene; sp, spinel.

Table 11: Amphibole (am)/clinopyroxene (cpx), phlogopite (phl)/clinopyroxene and phlogopite/amphibole partition coefficients of Kerguelen harzburgite and dunites

	Poikilitic harzburgite OB-93-5 am/cpx	Poikilitic harzburgites & phl-dunites phl/cpx		Am + phl-dunite MG-91-143 phl/cpx	Poikilitic harzburgite OB-93-5 phl/am
		average	range		
Sc	0·707	0·09	0·07–0·13	0·03	0·18
V	1·51	1·19	0·90–1·60	0·44	1·06
Co	1·75	3·02	2·65–3·95	2·87	2·24
Ni	2·48	5·05	4·40–6·25	5·30	2·52
Rb	109	3200	100–7700	1190	51
Ba	2212	12400	300–51000	497	23
Sr	2·29	0·83	0·50–1·30	1·10	0·43
Pb	3·01	3·59	1·40–8·70	26·56	1·99
Th	2·48	0·20	0·005–0·340	0·05	0·09
U	1·00	0·29	0·020–0·62	1·14	0·63
Nb	24·64	76·00	412·00–130·00	39·14	2·09
Ta	5·17	24·56	12·60–46·60	16·02	3·14
Ti	4·86	7·61	3·95–13·10	2·02	1·52
Zr	0·912	0·30	0·10–0·60	0·031	0·30
Hf	0·447	0·19	0·05–0·35	0·033	0·167
La	1·37	0·008	0·003–0·010	0·015	0·004
Ce	1·02	0·008	0·002–0·020	0·014	0·004
Nd	0·664	0·011	0·003–0·030	0·017	0·014
Sm	0·623	0·018	0·008–0·055	0·023	0·024
Eu	0·694	0·032	0·010–0·070	0·023	0·049
Gd	0·598	0·024	0·015–0·030	0·021	0·047
Dy	0·646	0·061	0·02–0·14	0·030	
Ho	0·600	0·071	0·021–0·16	0·036	0·083
Er	0·835	0·080	0·025–0·185	0·042	0·064
Yb	0·659	0·110	0·035–0·30	0·049	0·126
Lu	0·729	0·130	0·05–0·30	0·077	0·171
Y	0·698	0·013	0·002–0·035	0·005	0·048

Calculated mineral–melt partition coefficients

Data for trace element partitioning between olivine, orthopyroxene, spinel, amphibole, phlogopite and mafic silicate and carbonatitic melts are rare compared with those for clinopyroxene–melt partitioning (Green, 1994; Ionov *et al.*, 1997). We have calculated mineral–melt D values for these phases by multiplying the average mineral–clinopyroxene ratio for each element by clinopyroxene–melt partition coefficients from the literature. For harzburgite and phlogopite-bearing dunite we used the $D_{cpx/sil}$ (as discussed above); for the phlogopite + amphibole-bearing dunite MG-91-143 we used the $D_{cpx/carb\ melts}$ (as discussed above). We assumed that $D_{mineral/cpx}$ values at the subsolidus temperature are similar to those at near-liquidus temperature in basaltic systems. This assumption is controversial: some researchers have argued that temperature and mineral composition have little effect on D values (Ionov *et al.*, 1997; Johnson, 1998), and others have provided experimental data indicating the opposite (e.g. Green, 1994; Blundy *et al.*, 1998).

The calculated partition coefficients between olivine, opx, spinel and basic silicate melt are very low, except for $D^{Ti}_{opx/melt}$, $D^{Zr}_{sp/melt}$ and the $D^{Ti}_{sp/melt}$ (Table 12). $D_{opx/melt}$ values are very small for La and Ce but much greater for other REE. The values compare well with

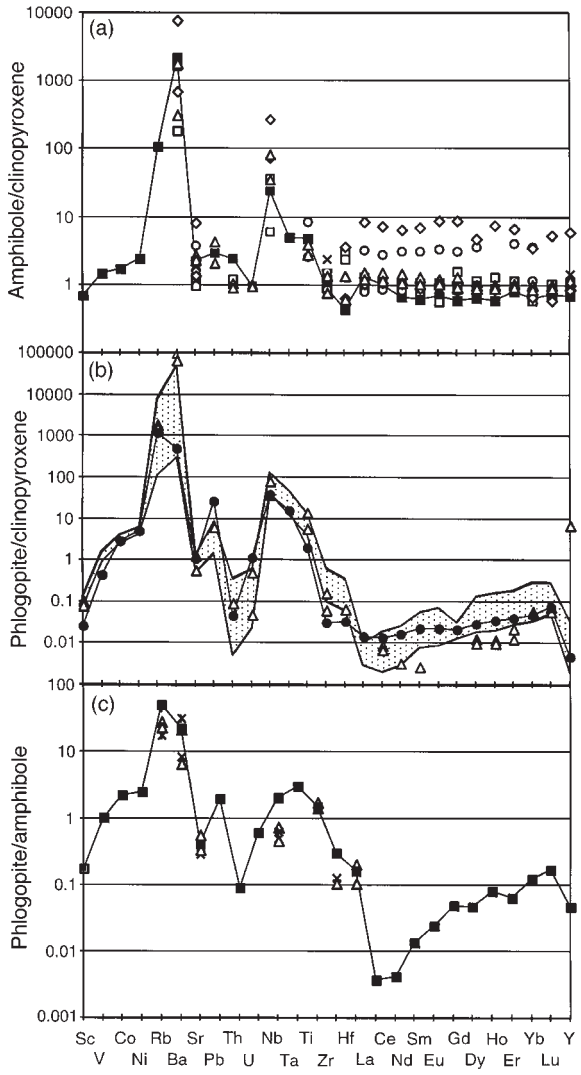

Fig. 8. (a) Amphibole–clinopyroxene partition coefficients (sample OB-93-5; ■); (b) phlogopite–clinopyroxene partition coefficients (dotted field, poikilitic harzburgites and phlogopite-bearing dunites; ●, phlogopite + amphibole-bearing dunite sample MG-91-143); (c) phlogopite–amphibole partition coefficients (sample OB-93-5, ■). Values from the literature: □, Chazot *et al.*, 1996; ◇, Witt-Eickschen & Harte, 1994; ○, Vannucci *et al.*, 1995; △, Ionov *et al.*, 1997; oblique cross, O'Reilly *et al.*, 1991; cross, Stosch & Lugmair, 1986; double cross, Zanetti *et al.*, 1996.

the GERM partition coefficient compilation (http://www-ep.es.llnl.gov/germ/partitioning.html).

Our estimates of phlogopite–mafic silicate melt partition coefficient for Rb, Ba, Th, U, Nb, Ta and Pb (Table 12) are larger than other published data (La Tourette *et al.*, 1995; Foley *et al.*, 1996; Ionov *et al.*, 1997; see Appendix). Values for Sr are smaller and those for Ti (Table 12) are similar to those of Ionov *et al.* (1997). Our $D^{Rb}_{phl/sil}$ agrees with the value of 8·2 calculated by Ionov *et al.* (1997). The *D* value for Ce agrees with that calculated by Ionov *et al.* (1997; *D* 0·0006) but values for other REE are systematically larger (Table 12 and Appendix). The experimental data of La Tourrette *et al.* (1995) for La and Nd, and the measured data of Foley *et al.* (1996) for Ce, are larger than our values. The partition coefficients between phlogopite from sample MG-91-143 and carbonatitic melt indicate that Rb (and probably Ba), Nb, Ta and Ti behave as compatible elements in this chemical system and that phlogopite is a good residence site for those trace elements (Table 12). *D* values for Zr and Hf are less than those for basic silicate melt. The *D* values for REE progressively increase from LREE to HREE.

The calculated partition coefficients between amphibole and mafic silicate melt are given in Table 12. Ba and Ti are concentrated in amphibole relative to melt; other trace elements display *D* values ranging from 0·010 (U) to 0·44 (Rb). The *D* values for REE increase from La to Eu with nearly constant values from Gd to Lu. The same trend has been observed by Chazot *et al.* (1996). Zr and Hf have similar partition coefficients but those for Ta are less than those for Nb (Table 12). *D* values for Pb are larger than those for Th and U. *D* values for Ba and Th are close to values proposed by Chazot *et al.* (1996); D^{Ba} up to 1·59 and Brenan *et al.* (1995); D^{Th} 0·017. *D* values for LREE and HREE agree with those of Chazot *et al.* (1996) and Witt-Eickschen & Harte (1994) but *D* values for MREE are smaller (Table 12). Although *D* values for Sr and Hf are less than literature values, those for Zr and Nb are similar to those obtained by Adam *et al.* (1993), Dalpe & Baker (1994), Witt-Eickschen & Harte (1994), Brenan *et al.* (1995), La Tourrette *et al.* (1995), Chazot *et al.* (1996) and Ionov *et al.* (1997).

Trace element residence sites

The trace element contents of constituent minerals (olivine + clinopyroxene + spinel ± orthopyroxene ± phlogopite ± amphibole) and their modal proportions can be used to calculate whole-rock compositions for comparison with the whole-rock analyses, to evaluate mass balance and the proportions of elements that reside in constituent minerals.

The clinopyroxene-poor lherzolite JGM-92-1c and the phlogopite-bearing-dunite MM-94-54 have incompatible trace element bulk-rock contents that can be easily explained by their constituent minerals, but all other samples display significant discrepancies between calculated and measured bulk-rock trace element compositions (Figs 9 and 10). Discrepancies are evident for Rb, Ba, Sr, Nb, Ta, Zr, Hf, Th, U, Pb and LREE; the MREE, HREE and transition trace elements are generally concordant. Samples that deviate from calculated trace element compositions contain veins and

Table 12: Orthopyroxene (opx)/mafic silicate melts (Sil), olivine (ol)/Sil and spinel (sp)/Sil partition coefficients calculated from Kerguelen protogranular harzburgites; phlogopite (phl)/Sil, phlogopite/carbonatitic melts (Carb) and amphibole (am)/Sil partition coefficients calculated from Kerguelen poikilitic harzburgites and dunites

	Protogranular harzburgites			Poikilitic harzburgites and phl-dunites		am + phl-dunite MG-91-143		Poikilitic harzburgite OB-93-5
	opx/Sil	ol/Sil	sp/Sil	phl/Sil		phl/Carb		am/Sil
Rb	0·0026	0·0013	0·0454	11·87	Rb	4·7588	Rb	0·4357
Ba	0·0008	0·0005	0·0052	5·24	Nb	3·9139	Ba	1·9909
Sr	0·0099	0·0075	0·0441	0·0655	Ta	2·4033	Sr	0·1813
Pb	0·0121	—	0·0796	0·2164	La	0·0010	Pb	0·2171
Th	—	0·0060	0·0023	0·0014	Ce	0·0013	Th	0·0149
U	0·0050	0·0182	—	0·0028	Sr	0·0879	U	0·0100
Nb	0·0010	—	0·0128	0·3629	Nd	0·0019	Nb	0·1232
Ta	—	—	0·0492	0·2255	Sm	0·0030	Ta	0·0517
Ti	0·1933	0·0150	0·8363	2·7853	Zr	0·0151	Ti	1·8660
Zr	0·0492	0·0190	0·1804	0·0348	Hf	0·0053	Zr	0·1113
Hf	0·0358	—	—	0·0476	Eu	0·0050	Hf	0·1144
La	0·0015	0·0017	—	0·0004	Ti	2·8671	La	0·0893
Ce	0·0051	0·0009	0·0081	0·0007	Gd	0·0056	Ce	0·0986
Nd	0·0475	—	—	0·0019	Dy	0·0087	Nd	0·1349
Sm	0·0634	—	—	0·0045	Y	0·0360	Sm	0·1800
Eu	0·0743	—	0·0859	0·0095	Er	0·0171	Eu	0·2269
Gd	0·0726	—	—	0·0096			Gd	0·2027
Dy	0·0522	—	—	0·0182			Dy	0·2428
Er	0·0542	0·0261	—	0·0192			Er	0·2941
Yb	0·0415	—	—	0·0330			Yb	0·2450
Lu	0·0732	—	—	0·0395			Lu	0·2552

patches of metasomatic phases that were not analysed. Harzburgite samples GM-92-501, OB-93-3 and OB-93-5 show variable proportion of veins and patches that contain feldspar, olivine, ilmenite, rutile and armalcolite and chromite (Grégoire *et al.*, 2000). However, harzburgite samples GM-92-453 and GM-92-502 display rare patches, which contain clinopyroxene ± carbonate ± chromite. Finally, phlogopite-bearing dunite samples GM-92-480 and MM-94-101 display few patches, which contain clinopyroxene ± amphibole ± biotite ± chromite ± rutile ± carbonate. We therefore conclude that metasomatic veins and patches contribute significantly to the Rb, Ba, Sr, Nb, Ta, Zr, Hf, Th, U, Pb and LREE contents of these seven peridotite samples. For example, a significant amount of Sr is probably hosted by feldspar, carbonate, phlogopite and amphibole occurring in the metasomatic veins and patches. Therefore, the major mineral phases (including the metasomatic phases) can account for the trace element budget without considering glass or fine-grained areas of metasomatic minerals. In addition, these samples do not show any significant trace element component in fluid and solid inclusions or at grain boundaries [compare with O'Reilly *et al.* (1991) and Eggins *et al.* (1998)]. These observations are consistent with those of Rosenbaum *et al.* (1996), who argued that fluid inclusions will dominate the incompatible element budget of typical mantle peridotite only if present in greater than sub-weight percent quantities.

Our mass balance calculations estimate the fractional contribution by specific mineral phases to the calculated bulk-rock composition in samples where the calculated composition is close to the bulk-rock analysis (clinopyroxene-poor lherzolite JGM-92-1c, harzburgite GM-92-453 and dunite samples MM-94-54, MM-94-101 and GM-92-480). Clinopyroxene is the dominant host of REE, Sr, Y, Zr and Th; opx and olivine host HREE, especially Yb and Lu (Fig. 11). Olivine, the dominant mineral phase, is the major host of Ni (and

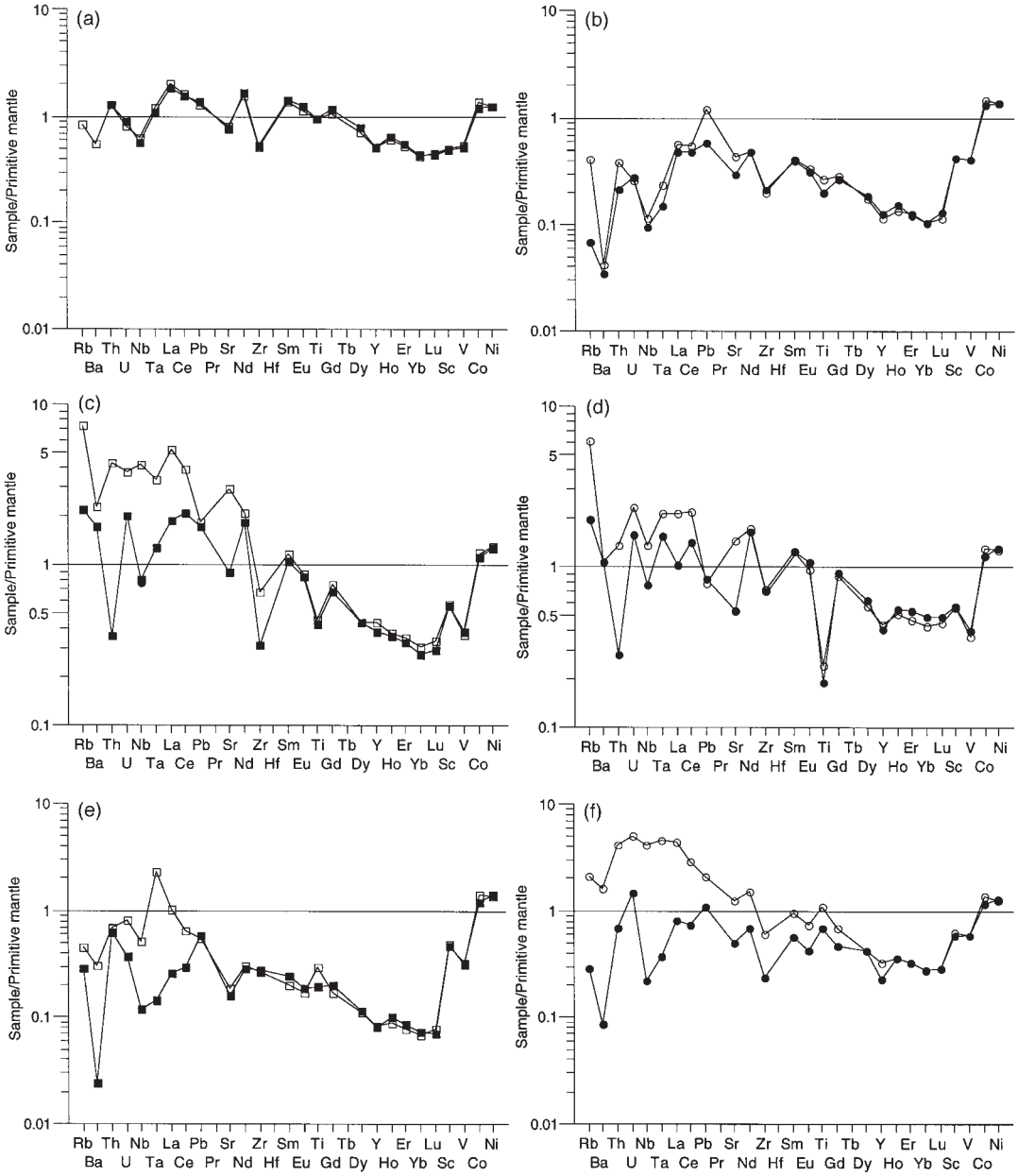

Fig. 9. Comparison between primitive mantle-normalized incompatible trace element patterns of measured and calculated bulk-rock compositions of Kerguelen poikilitic harzburgites and cpx-poor lherzolite (see text for explanation). Normalizing values after McDonough & Sun (1995). (a) sample JGM-92-1c; (b) sample GM-92-453; (c) sample OB-93-5; (d) sample OB-93-3; (e) sample GM-92-502; (f) sample GM-92-501, which is the richest in metasomatic veins and patches (see text for explanation). Open symbols, measured compositions; filled symbols, calculated compositions.

Co) as well as for Pb and Sc. Olivine, when present in high modal abundances, contributes significantly to bulk-rock Nb, Rb, Ba and Th contents (Fig. 11), despite its very low contents of these elements. Opx in harzburgite and clinopyroxene-poor lherzolite is an important host for Sc, Ti, V, Zr, Y, Rb and HREE, again because of its high modal proportion in these rocks. In dunite samples, phlogopite is the principal residence site for Rb, Ba, Nb and Ti, but not Zr or Pb. Spinel hosts significant amounts of V and Ti. Despite its relatively large D^{HFSE} compared with olivine, clinopyroxene and orthopyroxene, spinel does not contribute much of the bulk-rock budget of Nb, Ta, Zr and Ti, owing to its small modal abundance.

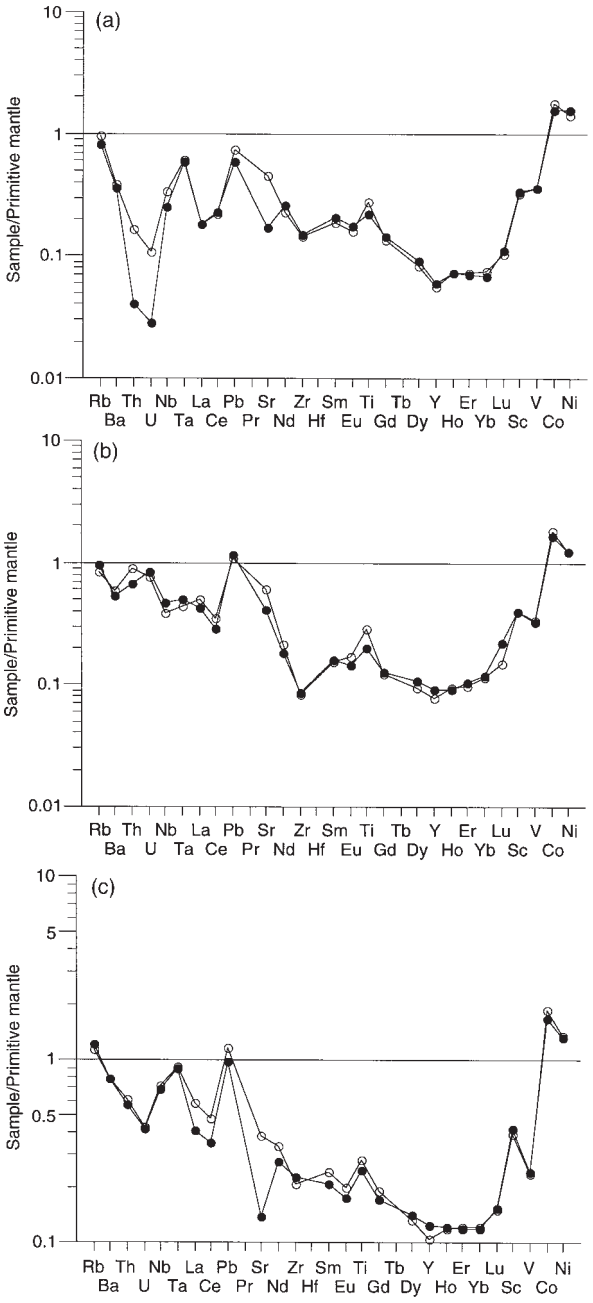

Fig. 10. Comparison between primitive mantle-normalized incompatible trace element patterns of measured and calculated bulk-rock compositions of Kerguelen clinopyroxene + phlogopite-bearing dunites (see text for explanation). Normalizing values after McDonough & Sun (1995). (a) Sample GM-92-480; (b) sample MM-94-54; (c) sample MM-94-101. ○, Measured compositions; ●, calculated compositions.

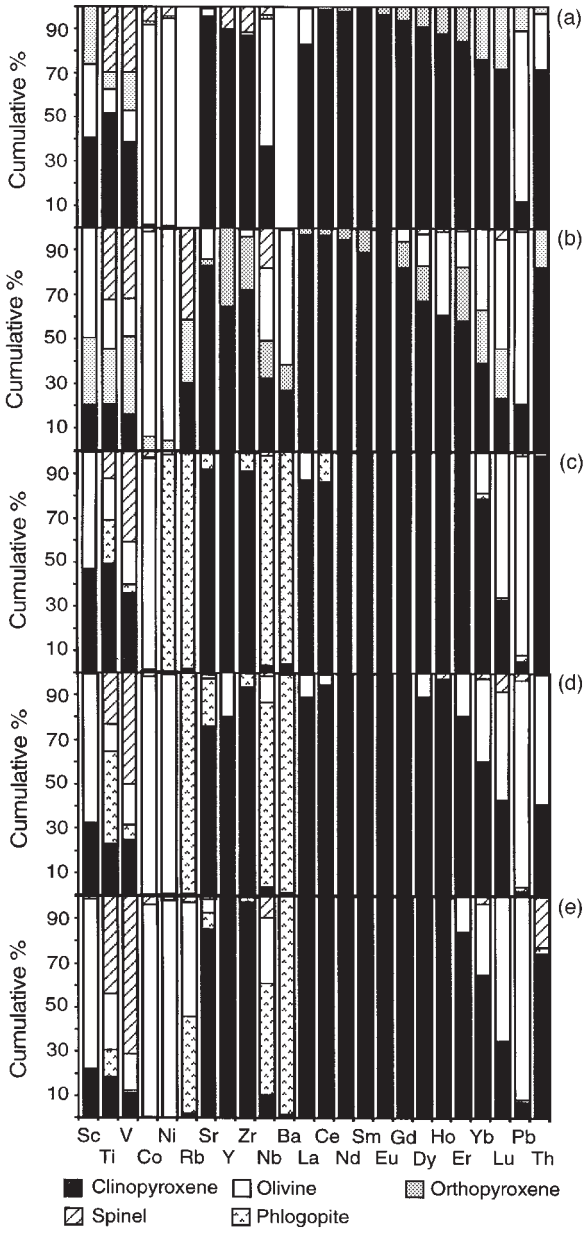

Fig. 11. Relative contributions of the constituent mineral phases to the trace-element budgets for (a) cpx-poor lherzolite (JGM-92-1c); (b) harzburgite GM-92-453; (c,d and e) dunites MM-94-54, MM-94-101 and GM-92-480, respectively.

SUMMARY AND CONCLUSIONS

The trace element signatures of mantle xenoliths indicate that pervasive mantle metasomatism by melts with intraplate alkali mafic silicate affinities occurred on a large scale in the Kerguelen lithospheric mantle. The inferred metasomatic fluids range from highly alkaline mafic silicate magmas to CO_2-rich silicate melts ('carbonatitic'). Carbonatitic mantle metasomatism beneath the Kerguelen archipelago (Schiano *et al.*, 1994; Mattielli, 1996; Mattielli *et al.*, 1999) is probably restricted in its impact. The dominant metasomatic agent is the mantle equivalent of highly alkaline silicate magmas that have erupted in

the Kerguelen Archipelago and are observed as late-stage 'lamprophyric dykes'.

The petrological and geochemical characteristics of the two types of Kerguelen harzburgites and clinopyroxene-poor lherzolite can be explained by a two-stage process related to the origin and evolution of the Kerguelen archipelago. In stage I, partial melting associated with the formation of the Kerguelen oceanic lithosphere in the vicinity of the South East Indian Ridge results in harzburgite. In stage II, reaction between these harzburgitic residues and various alkaline mafic silicate to carbonatitic melts reflects a contribution from the Kerguelen mantle plume. Anhydrous dunites may also have formed by reaction between harzburgite and basaltic melts in the upper mantle during the early tholeiitic–transitional magmatic activity that formed the archipelago. Later metasomatism of the anhydrous dunites by alkaline mafic silicate to carbonatitic melts may then be related to the activity of the Kerguelen mantle plume in the within-plate setting of the islands.

The trace element budgets of the Kerguelen mantle rocks can be quantitatively accounted for by the major mineral phases in samples that do not contain significant metasomatic veins and patches. In these samples there is no significant concentration of trace elements on grain boundaries or in fluid and solid inclusions. This result is similar to that obtained by O'Reilly *et al.* (1991) for a more restricted element set for 12 xenoliths from western Victoria (Australia) and by Eggins *et al.* (1998) for two mantle peridotites from southeastern Australia.

Our results emphasize the major role of clinopyroxene as host for trace elements such as REE, Sr, Y, Zr and Th. Spinel is an important residence site of V, Pb, Sc and Ti, but its small modal abundance indicates that it has but a small effect on the trace element budget of these rocks. Olivine may be an important residence site of Pb and Sc, despite its paucity of trace elements, because it constitutes the major part of modes. If orthopyroxene is a major constituent, it may contribute significantly to rock budgets for Sc, V, Zr and Ti, as has been proposed by Rampone *et al.* (1991) and discussed by Xu *et al.* (2000). Phlogopite contributes to rock budgets for Ba, Nb, Ta and Ti.

ACKNOWLEDGEMENTS

This work has been made possible by the generous assistance and technical expertise of N. J. Pearson, A. Sharma and C. Lawson (GEMOC Geochemical Analysis Unit). We thank T. H. Green, D. A. Ionov and N. J. Pearson for their helpful comments and English improvement. We very much appreciate the thoughtful and constructive reviews by Doug Smith, S. Sorensen and D. G. Pearson, which helped to improve the paper and clarify presentation. This work has been supported by Macquarie University Research Fellowship and Grant Schemes (M.G.), Australian Research Council Large and Small Grants (S.Y.O'R.) and the ARC International Fellowship Scheme (M.G.). Bertrand Moine acknowledges support from the 'Région Rhône-Alpes, Programme EMERGENCE'. We also thank the following institutions for their support: the French Polar Research and Technology Institute (IFRTP, Brest, France), the French CNRS UMR-6524, the French Ministry of Education and Research and the University Jean Monnet (St Etienne, France). This is Publication 175 of the ARC National Key Centre for the Geochemical Evolution and Metallogeny of Continents (GEMOC).

REFERENCES

Adam, J., Green, T. H. & Sie, S. H. (1993). Proton microprobe determined partitioning of Rb, Sr, Ba, Y, Zr, Nb and Ta between experimentally produced amphiboles and silicate melts with variable F contents. *Chemical Geology* **109**, 29–49.

Baker, J., Chazot, G., Menzies, M. & Thirlwall, M. (1998). Metasomatism of the shallow mantle beneath Yemen by the Afar plume—implications for mantle plumes, flood volcanism, and intraplate volcanism. *Geology* **26**, 431–434.

Ballhaus, C., Berry, R. F. & Green, D. H. (1991). High pressure experimental calibration of the olivine–orthopyroxene–spinel oxygen geobarometer: implications for the oxidation state of the upper mantle. *Contributions to Mineralogy and Petrology* **107**, 27–40.

Blundy, J. D., Robinson, J. A. C. & Wood, B. J. (1998). Heavy REE are compatible in clinopyroxene on the spinel lherzolite solidus. *Earth and Planetary Science Letters* **160**, 493–504.

Bodinier, J. L., Dupuy, C. & Dostal, J. (1988). Geochemistry and petrogenesis of Eastern Pyrenean peridotites. *Geochimica et Cosmochimica Acta* **52**, 2893–2907.

Bodinier, J. L., Menzies, M. A. & Thirlwall, M. F. (1991). Continental to oceanic mantle transition–REE and Sr–Nd isotopic geochemistry of the Lanzo Lherzolite Massif. *Journal of Petrology*, special issue, Orogenic Lherzolites and Mantle Processes, 175–189.

Brenan, J. M., Shaw, H. F., Ryerson, F. J. & Phinney, D. L. (1995). Experimental determination of trace-element partitioning between pargasite and a synthetic hydrous andesitic melt. *Earth and Planetary Science Letters* **135**, 1–11.

Brey, G. P. & Köhler, T. (1990*a*). Geothermobarometry in four-phase lherzolites. I: Experimental results from 10 to 60 kbar. *Journal of Petrology* **31**, 1313–1352.

Brey, G. P. & Köhler, T. (1990*b*). Geothermobarometry in four-phase lherzolites. II. New thermobarometers, and practical assessment of existing thermobarometers. *Journal of Petrology* **31**, 1353–1378.

Brown, G. M., Pinsent, R. H. & Coisy, P. (1980). The petrology of spinel-peridotite xenoliths from the Massif Central, France. *American Journal of Science* **280A**, 471–496.

Chalot-Prat, F. & Boullier, A.-M. (1997). Metasomatism in the subcontinental mantle beneath the Eastern Carpathians (Romania): new evidence from trace element geochemistry. *Contributions to Mineralogy and Petrology* **129**, 284–307.

Chazot, G., Menzies, M. A., Harte, B. & Mattey, D. (1994). Carbonatite metasomatism and melting of the Arabian lithosphere: evidence from oxygen isotopes and trace element composition of spinel lherzolites. *Mineralogical Magazine* **58A**, 167–168.

Chazot, G., Menzies, M. & Harte, B. (1996). Determination of partition coefficients between apatite, clinopyroxene, amphibole, and melt in natural spinel lherzolites from Yemen: implications for wet melting of the lithospheric mantle. *Geochimica et Cosmochimica Acta* **60**, 423–437.

Clague, D. A. (1988). Petrology of ultramafic xenoliths from Loihi Seamount, Hawaii. *Journal of Petrology* **29**, 1161–1186.

Coffin, M. F. & Eldhom, O. (1993). Scratching the surface: estimating dimensions of large igneous provinces. *Geology* **21**, 515–518.

Coisy, P. & Nicolas, A. (1978). Structure et géodynamique du manteau supérieur sous le Massif Central (France) d'après l'étude des enclaves des basaltes. *Bulletin de Minéralogie* **4**, 424–436.

Dalpe, C. & Baker, D. R. (1994). Partition coefficients for rare-earth elements between calcic amphibole and Ti-rich basanitic glass at 1·5 GPa, 1100°C. *Mineralogical Magazine* **58A**, 207–208.

Downes, H. & Dupuy, C. (1987). Textural, isotopic and REE variation in spinel peridotite xenoliths, Massif Central, France. *Earth and Planetary Science Letters* **82**, 121–135.

Downes, H., Bodinier, J. L., Thirwall, M. F., Lorand, J. P. & Fabriès, J. (1991). REE and Sr–Nd isotopic geochemistry of Eastern Pyrenean peridotite massifs: sub-continental lithospheric mantle modified by continental magmatism. *Journal of Petrology*, special issue, Orogenic Lherzolites and Mantle Processes, 97–116.

Eggins, S. M., Woodhead, J. D., Kinsley, L., Mortimer, G. E., Sylvester, P., McCulloch, M. T., Hergt, J. M. & Handler, M. R. (1997). A simple method for the precise determination of ≥40 trace elements in geological samples by ICP-MS using enriched isotope internal standardisation. *Chemical Geology* **134**, 311–326.

Eggins, S. M., Rudnick, R. L. & McDonough, W. F. (1998). The composition of peridotites and their minerals: a laser-ablation ICP-MS study. *Earth and Planetary Science Letters* **154**, 53–71.

Elthon, D. (1993). Crystallization of mid-ocean ridge basalts. *European Journal of Mineralogy* **5**, 1025–1037.

Fabriès, J. (1979). Spinel–olivine geothermometry in peridotites from ultramafic complexes. *Contributions to Mineralogy and Petrology* **69**, 329–336.

Fabriès, J., Bodinier, J. L., Dupuy, C., Lorand, J. P. & Benkerrou, C. (1989). Evidence for modal metasomatism in the orogenic spinel lherzolite body from Caussou (Northeastern Pyrenees, France). *Journal of Petrology* **30**, 176–199.

Foley, S., Jackson, S. E., Fryer, B. J., Greenough, J. D. & Jenner, G. A. (1996). Trace element partition coefficients for clinopyroxene and phlogopite in an alkaline lamprophyre from Newfoundland by LAM-ICP-MS. *Geochimica et Cosmochimica Acta* **60**, 629–638.

Frey, F. A. & Prinz, M. (1978). Ultramafic inclusions from San Carlos, Arizona. Petrologic and geochemical data bearing on their petrogenesis. *Earth and Planetary Science Letters* **38**, 139–176.

Gautier, I., Weis, D., Mennessier, J. P., Vidal, P., Giret, A. & Loubet, M. (1990). Petrology and geochemistry of the Kerguelen Archipelago basalts (South Indian Ocean): evolution of the mantle sources from ridge to intraplate position. *Earth and Planetary Science Letters* **100**, 59–76.

Giret, A. (1993). Les étapes magmatiques de l'édification des îles Kerguelen. *Bulletin de la Société Géologique de France*, Bulletin APBG, numéro spécial, 273–282.

Giret, A., Grégoire, M., Cottin, J. Y. & Michon, G. (1997). The Kerguelen islands: the third type of oceanic islands. In: Ricci, C. A. (ed.) *The Antarctic Region: Geological Evolution and Processes*. Siena: Terra Antarctica Publications, pp. 735–741.

Green, T. H. (1994). Experimental studies of trace element partitioning applicable to igneous petrogenesis—Sedona 16 years later. *Chemical Geology* **117**, 1–36.

Green, T. H., Adam, J. & Sie, S. H. (1992). Trace element partitioning between silicate minerals and carbonatite at 25 kbar and application to mantle metasomatism. *Mineralogy and Petrology* **46**, 179–184.

Grégoire, M. (1994). Pétrologie des enclaves ultrabasiques et basiques des îles Kerguelen (T.A.A.F.). Les contraintes minéralogiques et thermobarométriques et leurs implications géodynamiques. Thèse de doctorat, Université Saint Etienne, 253 pp.

Grégoire, M., Mattielli, N., Nicollet, C., Cottin, J. Y., Leyrit, H., Weis, D., Shimizu, N. & Giret, A. (1994). Oceanic mafic granulite from the Kerguelen Archipelago. *Nature* **367**, 360–363.

Grégoire, M., Lorand, J. P., Cottin, J. Y., Giret, A., Mattielli, N. & Weis, D. (1997). Petrology of Kerguelen mantle xenoliths: evidence of a refractory oceanic mantle percolated by basaltic melts beneath the Kerguelen archipelago. *European Journal of Mineralogy* **9**, 1085–1100.

Grégoire, M., Cottin, J. Y., Giret, A., Mattielli, N. & Weis, D. (1998). The metaigneous xenoliths from Kerguelen archipelago: evidence of a continent nucleation in an oceanic setting. *Contributions to Mineralogy and Petrology* **133**, 259–283.

Grégoire, M., Lorand, J. P., O'Reilly, S. Y. & Cottin, J. Y. (2000). Armalcolite-bearing, Ti-rich metasomatic assemblages in harzburgitic xenoliths from the Kerguelen Archipelago: implications for the oceanic mantle budget of high-field strength elements. *Geochimica et Cosmochimica Acta* (in press).

Hart, S. R. & Dunn, T. (1993). Experimental cpx/melt partitioning of 24 trace elements. *Contributions to Mineralogy and Petrology* **113**, 1–8.

Hassler, D. R. & Shimizu, N. (1998). Osmium isotopic evidence for ancient subcontinental lithospheric mantle beneath the Kerguelen Islands, southern Indian Ocean. *Science* **280**, 418–421.

Hauri, E. H., Shimizu, N., Dieu, J. J. & Hart, S. R. (1993). Evidence for hotspot-related carbonatite metasomatism in the oceanic upper mantle. *Nature* **365**, 221–227.

Ionov, D. A., Kramm, U. & Stosch, H.-G. (1993). Evolution of the upper mantle beneath the southern Baikal rift zone: a Sr–Nd isotope study of xenoliths from the Bartoy volcanoes. *Contributions to Mineralogy and Petrology* **111**, 235–247.

Ionov, D. A., Griffin, W. L. & O'Reilly, S. Y. (1997). Volatile-bearing minerals and lithophile trace elements in the upper mantle. *Chemical Geology* **141**, 153–184.

Irving, A. J. & Frey, F. A. (1984). Trace element abundances in megacrysts and their host basalts: constraints on partition coefficients and megacryst genesis. *Geochimica et Cosmochimica Acta* **47**, 1201–1221.

Jagoutz, E., Palme, H., Baddenhauser, H., Blum, K., Cendales, M., Dreibus, G., Spettel, B., Lorenz, V. & Wänke, H. (1979). The abundance of major, minor and trace elements in the Earth's mantle as derived from primitive ultramafic nodules. *Proceedings of the 10th Lunar and Planetary Science Conference*. *Geochimica et Cosmochimica Acta Supplement* 2031–2050.

Johnson, K. T. M. (1998). Experimental determination of partition coefficients for rare earth and high-field-strength elements between clinopyroxene, garnet, and basaltic melt at high pressures. *Contributions to Mineralogy and Petrology* **133**, 60–68.

Johnson, K. T. M., Dick, H. J. B. & Shimizu, N. (1990). Melting in the oceanic upper mantle: an ion microprobe study of diopsides in abyssal peridotites. *Journal of Geophysical Research* **95**, 2661–2678.

Klemme, S., Van der Laan, S. R., Foley, S. F. & Günther, D. (1995). Experimentally determined trace and minor element partitioning between clinopyroxene and carbonatite melt under mantle conditions. *Earth and Planetary Science Letters* **133**, 439–448.

Kostopoulos, D. K. (1991). Melting of the shallow upper mantle: a new perspective. *Journal of Petrology* **32**, 671–699.

La Tourrette, T., Hervig, R. L. & Holloway, J. R. (1995). Trace element partitioning between amphibole, phlogopite, and basanite melt. *Earth and Planetary Science Letters* **135**, 13–30.

Leyrit, H. (1992). Kerguelen: cartographie et magmatologie des presqu'îles Jeanne d'Arc et Ronarc'h. Place des laves différenciées. Thèse d'Université, Université Paris XI–Orsay, 236 pp.

Longerich, H. P., Jackson, S. E. & Gunther, D (1996). Laser ablation inductively-coupled plasma-mass spectrometric transient signal acquisition and analyte concentration calculation. *Journal of Atomic Spectrometry* **11**, 899–904.

Liu, C.-Q., Masuda, A. & Xie, G.-H. (1992). Isotope and trace-element geochemistry of alkali basalts and associated megacrysts from the Huangyishan volcano, Kuandian, Liaoning, NE China. *Chemical Geology* **97**, 219–231.

Mattielli, N. (1996). Magmatisme et métasomatismes associés au panache des Kerguelen: contribution de la géochimie des enclaves basiques et ultrabasiques. Doctorat en Sciences Géologiques et Minéralogiques, Université Libre de Bruxelles, 213 pp.

Mattielli, N., Weis, D., Grégoire, M., Mennessier, J. P., Cottin, J. Y. & Giret, A. (1996). Kerguelen basic and ultrabasic xenoliths: evidence for long-lived Kerguelen hotspot activity. *Lithos* **37**, 261–280.

Mattielli, N., Weis, D., Scoates, J. S., Shimizu, N., Mennessier, J. P., Grégoire, M., Cottin, J. Y. & Giret, A. (1999). Evolution of heterogeneous lithospheric mantle in a plume environment beneath the Kerguelen Archipelago. *Journal of Petrology* (in press).

McDonough, W. F. & Sun, S.-s. (1995). The composition of the Earth. *Chemical Geology* **120**, 223–253.

Moine, B., Sheppard, S. M. F., Cottin, J. Y., Grégoire, M., O'Reilly, S. Y. & Giret, A. (2000). Trace element and isotopic (D/H) characteristics of amphibole- and/or phlogopite-bearing ultramafic–mafic xenoliths from Kerguelen islands (TAAF, South Indian Ocean). *European Journal of Mineralogy* (in press).

Mysen, B. O. & Kushiro, I. (1977). Compositional variations of coexisting phases with degree of melting of peridotite in the upper mantle. *American Mineralogist* **62**, 843–845.

Navon, O. & Stolper, E. (1987). Geochemical consequences of melt percolation: the upper mantle as a chromatographic column. *Journal of Geology* **95**, 285–307.

Nixon, P. H. (1987). *Mantle Xenoliths*. Chichester: John Wiley.

Nixon, P. H., Mitchell, R. H. & Rogers, N. W. (1980). Petrogenesis of alnöitic rocks from Malaita, Solomon Islands. *Mineralogical Magazine* **43**, 587–596.

Norman, M. D. (1998). Melting and metasomatism in the continental lithosphere: laser ablation ICPMS analysis of minerals in spinel lherzolites from eastern Australia. *Contributions to Mineralogy and Petrology* **130**, 240–255.

Norman, M. D., Pearson, N. J., Sharma, A. & Griffin, W. L. (1996). Quantitative analysis of trace elements in geological materials by laser ablation ICPMS: instrumental operating conditions and calibration values of NIST glasses. *Geostandards Newsletter* **20**, 247–261.

O'Reilly, S. Y. & Griffin, W. L. (1988). Mantle metasomatism beneath western Victoria, Australia: I. Metasomatic processes in Cr-diopside lherzolites. *Geochimica et Cosmochimica Acta* **52**, 433–457.

O'Reilly, S. Y. & Griffin, W. L. (1996). 4-D lithosphere mapping: methodology and examples. *Tectonophysics* **262**, 1–18.

O'Reilly, S. Y., Griffin, W. L. & Ryan, C. G. (1991). Residence of trace elements in metasomatized spinel lherzolite xenoliths: a proton microprobe study. *Contributions to Mineralogy and Petrology* **109**, 98–113.

Pouchou, J. L. & Pichoir, F. (1984). A new model for quantitative X-ray microanalysis. Part 1: application to the analysis of homogeneous samples. *Recherche Aérospatiale* **5**, 13–38.

Presnall, D. C., Dixon, S. A., Dixon, J. R., O'Donell, T. H., Brenner, N. L., Schrock, R. L. & Dycus, D. W. (1978). Liquidus phase relations on the join diopside–forsterite–anorthite from 1 atm to 20 kbar: their bearing on the generation and crystallization of basaltic magma. *Contributions to Mineralogy and Petrology* **66**, 203–220.

Rampone, E., Bottazzi, P. & Ottolini, L. (1991). Complementary Ti and Zr anomalies in orthopyroxene and clinopyroxene from mantle peridotites. *Nature* **354**, 518–520.

Rock, N. M. S. (1987). The nature and origin of lamprophyres: an overview. In: Fitton, J. G. & Upton, B. G. J. (eds) *Alkaline Igneous Rocks. Geological Society, London, Special Publication* **30**, 191–226.

Rosenbaum, J. M., Zindler, A. & Rubenstone, J. L. (1996). Mantle fluids: evidence from fluid inclusions. *Geochimica et Cosmochimica Acta* **60**, 3229–3252.

Sachtleben, T. & Seck, H. A. (1981). Chemical control of Al-solubility in orthopyroxene and its implications on pyroxene geothermometry. *Contributions to Mineralogy and Petrology* **78**, 157–165.

Schiano, P., Clocchiatti, R., Shimizu, N., Weis, D. & Mattielli, N. (1994). Cogenetic silica-rich and carbonate-rich melts trapped in mantle minerals in Kerguelen ultramafic xenoliths: implications for metasomatized upper mantle. *Earth and Planetary Science Letters* **111**, 69–82.

Sen, G. (1987). Xenoliths associated with the Hawaiian Hot Spot. In: Nixon, P. H. (ed.) *Mantle Xenoliths*. Chichester: John Wiley, pp. 359–375.

Sen, G., Frey, F. A., Shimizu, N. & Leeman, W. P. (1993). Evolution of the lithosphere beneath Oahu, Hawaii: rare earth element abundance in mantle xenoliths. *Earth and Planetary Science Letters* **119**, 53–69.

Siena, F., Beccaluva, L., Coltorti, M., Marchesi, S. & Morra, V. (1991). Ridge to hot-spot evolution of the Atlantic lithosphere mantle: evidence from Lanzarote peridotite xenoliths (Canary Islands). *Journal of Petrology*, special issue, Orogenic Lherzolites and Mantle Processes, 255–270.

Stosch, H.-G. & Lugmair, G. W. (1986). Trace element and Sr and Nd isotope geochemistry of peridotite xenoliths from the Eifel (West Germany) and their bearing on the evolution of the subcontinental lithosphere. *Earth and Planetary Science Letters* **80**, 281–298.

Sun, S. S. & McDonough, W. F. (1989). Chemical and isotopic systematics of oceanic basalts: implications for mantle composition and processes. In: Saunders, A. D. & Norry, M. J. (eds) *Magmatism in the Ocean Basins. Geological Society, London, Special Publication* **42**, 313–346.

Vannucci, R., Piccardo, G. B., Rivalenti, G., Zanetti, A., Rampone, E., Ottolini, L., Oberti, R., Mazzucelli, M. & Bottazzi, P. (1995). Origin of LREE-depleted amphiboles in the subcontinental mantle. *Geochimica et Cosmochimica Acta* **59**, 255–269.

Weis, D. & Frey, F. A. (1996). Role of the Kerguelen Plume in generating the eastern Indian Ocean seafloor. *Journal of Geophysical Research* **101**, 13831–13849.

Weis, D., White, W. M., Frey, F. A., Duncan, R. A., Fisk, M. R., Dehn, J., Ludden, J., Saunders, A. & Storey, M. (1992). The influence of mantle plume in generation of Indian oceanic crust. Synthesis of results from scientific drilling in the Indian Ocean. *Geophysical Monograph, American Geophysical Union* **70**, 57–89.

Weis, D., Frey, F. A., Leyrit, H. & Gautier, I. (1993). Kerguelen Archipelago revisited: geochemical and isotopic study of the S.E. Province lavas. *Earth and Planetary Science Letters* **118**, 101–119.

Witt-Eickschen, G. & Harte, B. (1994). Distribution of trace elements between amphibole and clinopyroxene from mantle peridotites of the Eifel (Western Germany): an ion-microprobe study. *Chemical Geology* **117**, 235–250.

Woolley, A. R. & Kempe, D. R. C. (1989). Carbonatites: nomenclatures, average chemical compositions, and element distribution. In: Bell, K. (ed.) *Carbonatites: Genesis and Evolution*. London: Unwin Hyman, pp. 1–14.

Xu, Y., Menzies, M. A., Vroon, P., Mercier, J.-C. & Lin, C. (1998). Texture–temperature–geochemistry relationships in the upper mantle as revealed from spinel peridotite xenoliths from Wangqing, NE China. *Journal of Petrology* **39**, 469–493.

Xu, X., O'Reilly, S. Y., Griffin, W. L. & Zhou, X. (2000). Genesis of young lithospheric mantle in southeastern China: a LAM-ICPMS trace element study. *Journal of Petrology* **41**, 111–148.

Yagi, K., Ishikawa, H. & Kojima, M. (1975). Petrology of a lamprophyre sheet in Tanegashima Island. Kagoshima prefecture, Japan. *Journal of Japanese Association of Mineralogy, Petrology and Economic Geology* **70**, 213–224.

Yang, H.-Y., Frey, F. A., Weis, D., Giret, A., Pyle, D. & Michon, G. (1998). Petrogenesis of the flood basalts forming the Northern Kerguelen Archipelago: implications for the Kerguelen Plume. *Journal of Petrology* **39**, 711–748.

Zanetti, A., Vannucci, R., Bottazzi, P., Oberti, R. & Ottolini, L. (1996). Infiltration metasomatism at Lherz as monitored by systematic ion-microprobe investigations close to a hornblendite vein. *Chemical Geology* **134**, 113–133.

APPENDIX A

Table A1: Type, paragenesis and provenance of Kerguelen mantle xenolith samples (locality numbers refer to Fig. 1)

Sample	Type	Paragenesis	Provenance
OB-93-58	Protogranular harzburgite	ol-opx-cpx-sp	Val Studer, 5
OB-93-279	Protogranular harzburgite	ol-opx-cpx-sp	Mont Trapèze, 7
BOB-93-666	Protogranular harzburgite	ol-opx-cpx-sp	Port Kirk, 8
OB-93-426	Protogranular harzburgite	ol-opx-cpx-sp	Dôme Rouge, 1
OB-93-67b	Protogranular harzburgite	ol-opx-cpx-sp	Val Studer, 5
OB-93-22	Poikilitic harzburgite	ol-opx-cpx-sp	Mont du Chateau, 6
GM-92-453	Poikilitic harzburgite	ol-opx-cpx-sp	Trièdre, 2
GM-92-502	Poikilitic harzburgite	ol-opx-cpx-sp	Pointe Suzanne, 4
GM-92-501	Poikilitic harzburgite	ol-opx-cpx-sp	Pointe Suzanne, 4
OB-93-3	Poikilitic harzburgite	ol-opx-cpx-sp-phl	Mont du Chateau, 6
OB-93-5	Poikilitic harzburgite	ol-opx-cpx-sp-am-phl	Mont du Chateau, 6
JGM-92-1c	Poikilitic cpx-poor lherzolite	ol-opx-cpx-sp	Ravin du Mica, 5
MG-91-260	Poikilitic harzburgite	ol-opx-cpx-sp	Pointe Suzanne, 4
GM-92-468	Phlogopite-bearing dunite	ol-cpx-sp-phl	Trièdre, 2
GM-92-480	Phlogopite-bearing dunite	ol-cpx-sp-phl	Trièdre, 2
BOB-93-640.1	Phlogopite-bearing dunite	ol-cpx-sp-phl	Capitole, 9
MM-94-54	Phlogopite-bearing dunite	ol-cpx-sp-phl	Vallée Ring, 10
MM-94-101	Phlogopite-bearing dunite	ol-cpx-sp-phl	Vallée Ring, 10
MG-91-143	Amphibole + phlogopite-bearing dunite	ol-cpx-sp-phl-am	Val Phonolite, 3

APPENDIX B

Table A2: Compilation of phlogopite(phl)/mafic silicate melt (Sil) and amphibole (am)/mafic silicate melt partition coefficients from the literature

Phl/Sil	Ionov *et al.* (1997)	La Tourette *et al.* (1995)	Foley *et al.* (1996)	Adam *et al.* (1993)
Rb	8·2000	2·5000	5·2000	5·8000
Ba	48·0000	3·7000	3·5000	2·9000
Sr	0·1500	0·1600	0·1800	0·2200
Pb	—	0·0180	0·0070	—
Th	0·0005	0·0014	<0·015	—
U	—	0·0011	—	—
Nb	0·0810	0·0880	0·0850	0·1400
Ta	—	—	0·1070	0·1400
Ti	2·5000	1·8000	—	1·0000
Zr	0·0260	0·0170	0·0230	0·1300
Hf	0·0480	0·1900	—	—
La	—	0·0280	—	—
Ce	0·0006	—	0·0078	
Nd	0·0006	0·0120	—	—
Sm	0·0008	—	—	—
Eu	—	—	—	—
Gd	—	0·0160	—	—
Dy	0·0045	—	—	—
Er	0·0074	—	—	—
Yb	0·0230	—	—	—
Lu	0·0290	—	—	—

Am/Sil	Witt-Eickchen & Harte (1994)	Irving & Frey (1984)	Liu *et al.* (1992)	Ionov *et al.* (1997)	La Tourrette *et al.* (1995)
Rb	—	—	—	0·5300	0·2000
Ba	—	—	—	0·5400	0·1600
Sr	—	—	—	0·3200	0·3000
Pb	—	—	—	0·0300	0·0400
Th	—	—	—	0·0056	0·0039
U	—	—	—	—	0·0041
Nb	—	—	—	0·1400	0·1600
Ta	—	—	—	—	—
Ti	—	—	—	1·5000	1·3000
Zr	—	—	—	0·1800	0·1300
Hf	—	—	—	0·2900	0·3300
La	0·06–0·21 and 0·32–0·65	0·17	0·13	0·0610	0·0550
Ce	0·10–0·34 and 0·48–1·01	0·26	0·20	0·1140	0·0960
Nd	0·20–0·82 and 1·05–2·41	0·44	0·37	0·2200	0·2500
Sm	0·27–1·04 and 1·36–2·71	0·76	0·52	0·3300	—
Eu	0·32–1·03 and 2·14–3·91	0·88	0·65	0·3600	0·3200
Gd	0·46–0·72 and 2·20	0·86	0·61	0·3800	—
Dy	0·44–0·70 and 2·04	0·78	0·57	0·4100	—
Er	0·37–0·69 and 2·21	0·68	0·41	0·4200	0·5700
Yb	0·29–1·01 and 1·32–1·93	0·59	0·27	0·3900	—
Lu	0·27–1·25 and 2·02–3·03	0·51	0·21	0·4100	0·4300

Table A2: continued

Am/Sil	Chazot *et al.* (1996)	Dalpe & Baker (1994)	Adam *et al.* (1993)	Brenan *et al.* (1995)
Rb	—	0·220	0·2–0·6	0·140
Ba	0·171–1·592	0·278	0·3–0·6	0·120
Sr	0·079–0·101	0·376	0·24–0·38	0·280
Pb	—	—	—	0·120
Th	0·006–0·007	—	—	0·017
U	—	—	—	0·008
Nb	0·032–0·196	0·050	0·08	0·200
Ta	—	—	0·07–0·11	0·210
Ti	—	0·717	0·7–1·1	2·000
Zr	0·150–0·233	0·124	0·18–0·33	0·230
Hf	0·627–0·838	0·331	—	0·450
La	0·061–0·084	0·039	—	—
Ce	0·092–0·112	0·067	—	0·220
Nd	0·187–0·221	0·142	—	0·620
Sm	0·234–0·323	0·188	—	—
Eu	0·190–0·366	0·351	—	—
Gd	0·304–0·549	0·368	—	—
Dy	0·322–0·459	0·406	—	—
Er	0·297–0·430	0·362	—	—
Yb	0·220–0·301	0·349	—	1·250
Lu	0·331–0·380	0·246	—	—